J. Fluid Mech. (1988), *vol.* 192, *pp.* 249–286
Printed in Great Britain

Three-dimensional thermal cellular convection in rectangular boxes

By K. R. KIRCHARTZ† AND H. OERTEL JR‡

†Institut für Strömungslehre und Strömungsmaschinen, Universität (TH) Karlsruhe, West Germany

‡Institut für Theoretische Strömungsmechanik, DFVLR-AVA, Göttingen, West Germany

(Received 22 October 1986 and in revised form 26 June 1987)

The extension of the classic Rayleigh–Bénard problem of a horizontal layer heated from below to the three-dimensional convection in rectangular boxes is dealt with in this paper both numerically and experimentally. Also discussed is the influence of shear flows in tilted boxes and the transition to time-dependent oscillatory convection. Three-dimensional numerical simulations allow the calculation of stationary solutions and the direct simulation of oscillatory instabilities. We limited ourselves to laminar and transcritical flows. For studying the particular characteristics of three-dimensional convection in horizontal containers, we carefully selected two container geometries with aspect ratios of 10:4:1 and 4:2:1. The onset of steady cellular convection in tilted boxes is calculated by an iterative application of a combined finite-difference method and a Galerkin method. The appearance of longitudinal and transverse convection rolls is determined by means of interferometrical measuring techniques and is compared with the results of the linear stability theory. The spatial flow structure and the transition to oscillatory convection is calculated for selected examples in the range of supercritical Rayleigh numbers. Experimental investigations concerning the stability behaviour of the steady solutions with regard to time-dependent disturbances show a distinct influence of the Prandtl number and confirm the importance of nonlinear effects.

1. Introduction

Thermal convection is an important mechanism of mass and heat transfer in nature and technology. Numerous applications are found in geophysics and astrophysics, meteorology and many practical systems. Not only are the atmospheric structure of planets, the granulation of the sun, the earth's magnetic field and continental drift determined by thermal convection, but also energy storage in large containers, reactor safety and reactor waste storage, solar collectors, crystal growth for microprocessors, solid–liquid interface dynamics and microstructures in foundry and technology.

The convective mass and heat transfer is determined in a large number of the practical applications by the buoyancy force, diffusion and chemical reactions. The classic Rayleigh–Bénard problem of horizontal fluid layers heated from below offers a first approach to highly complex convective flow processes. This problem is characterized by the thermally unstable stratification in the gravitational field. The basic state is defined by the heat conduction. If the temperature difference between the horizontal boundaries exceeds a certain critical value, buoyancy-driven thermal cellular convection will begin, combined with an increase in the heat flux through the

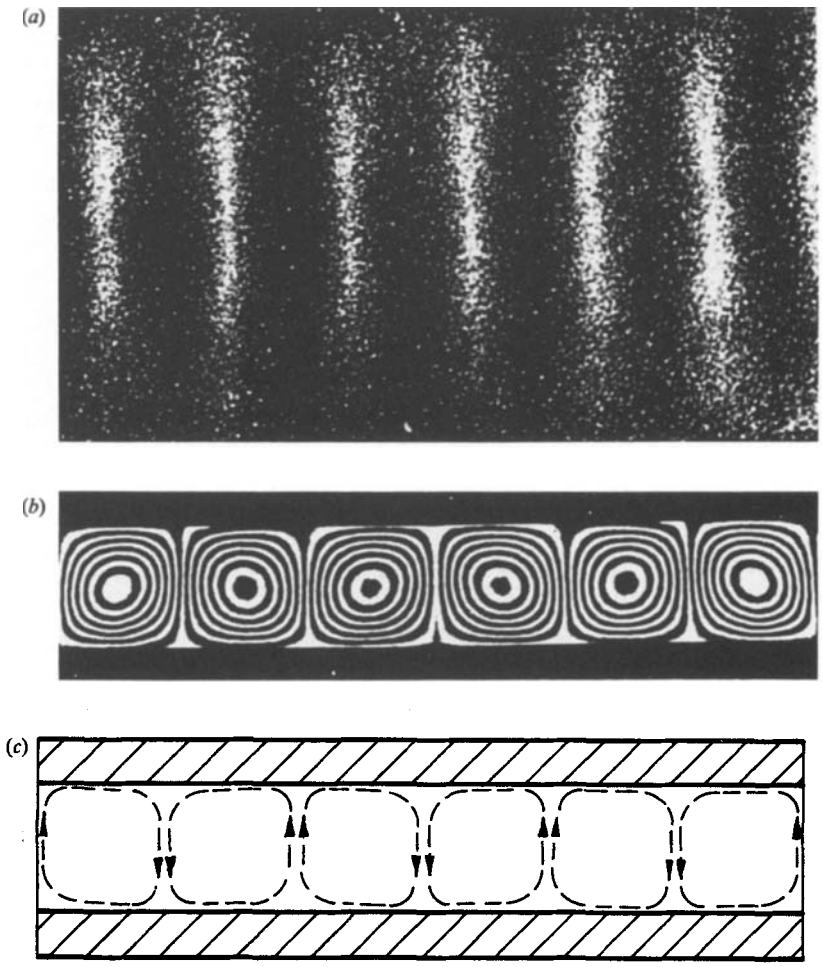

FIGURE 1. Planform of the Rayleigh–Bénard convection. (*a*) Top view, flow visualized by aluminium powder. (*b*) Differential interferogram. (*c*) Principle sketch.

fluid layer. Figure 1 shows the top view of the periodic flow field and a differential interferogram, which visualizes a cross-section of the flow pattern. If we assume rigid horizontal boundaries as in figure 1, longitudinal convection rolls appear. The fluid mechanical foundation of this classical stability problem, the derivation of the basic equations, the possible stationary and time-dependent convection configurations are described, for example, in the books and survey papers by Busse (1978), Chandrasekhar (1961), Gershuni & Zukhovitski (1976), Joseph (1976), Koschmieder (1974), Normand, Pomeau & Velarde (1977), Palm (1975), Roberts (1975), Swinney & Gollup (1981), Turner (1973) and Zierep & Oertel (1982).

The stability diagram from the linear stability theory (Chandrasekhar 1961) shows that thermal convection begins above a critical Rayleigh number with a characteristic wavenumber a_c. We call the Rayleigh–Bénard problem an absolutely unstable stability problem, since each local disturbance stretches progressively into the entire flow field. Accordingly, the temporally amplified stability theory describes the onset of cellular convection.

The basic phenomena of the Rayleigh–Bénard problem in an almost infinitely extended horizontal fluid layer are widely known. The influence of vertical boundaries and the flow pattern of thermal convection inside enclosures are of practical interest for engineering applications, in particular. This leads to the extension of the classic Rayleigh–Bénard problem to the convection in closed boxes. The stabilizing effect of vertical boundaries on the onset of cellular convection due to the additional friction is well understood within the framework of the linear stability theory. This is shown, for example, in the works of Catton (1978), Davis (1967), Stork & Müller (1972) and Zierep (1963).

Less known, however, is the three-dimensional structure of the nonlinear thermal cellular convection in containers and the area of influence of the vertical boundaries. There are conflicting results even about the wavelength selection of convection rolls in almost infinite horizontal fluid layers. Koschmieder (1974) defined this as a central question in the Rayleigh–Bénard problem. The three-dimensional reorientation of the convection rolls in containers with increasing heating rate has not been made at all clear. The experiments show an increase in the wavelength. Neither theoretical nor numerical simulation calculations can clarify this condition unequivocally. In particular, the highly complex structure of time-dependent oscillatory convection in boxes and the transition to thermal turbulence have been little investigated. (See, for example, the publications of Curry *et al.* 1984 and Kolodner *et al.* 1986). However, oscillatory instabilities in boxes proceed differently from Busse's (1978, 1981) published results in infinitely extensive layers, in the particular aspect of the controlled initial condition because here the flow configuration is mainly determined by the boundary conditions. The great number of possible bifurcation solutions dependent on the initial and boundary conditions increases. The limited geometry imposes an additional order principle. This has a quite decisive influence on the transition to time-dependent convection.

The convection in tilted boxes is an important extension of the Rayleigh–Bénard problem, and has both basic and practical significance. In a very simple manner, it permits the study of the combined action of shear flows and thermal instabilities. This has practical significance for the understanding of convective processes, including those in the earth's atmosphere, oceans and seas. Convection in tilted boxes gains particular technical importance for the thermal design of solar energy collectors. Accordingly there have been a large number of articles published on this subject; the common goal of most investigations has been the determination of the Nusselt number as a function of the relevant parameters (Rayleigh number, angle of inclination and aspect ratio).

The fluid mechanical aspects of convection in tilted geometries have been less investigated, particularly the complex stability mechanisms which, depending on the respective characteristic non-dimensional parameters, determine the flow structure and thereby help to interpret the functional dependence of the heat flux on the important parameters.

A number of articles are important for discussing these problems. Unny (1972) and Hollands & Konicek (1973) have theoretically and experimentally determined the basic flow's onset of instability in quasi-infinitely extended layers. Ruth *et al.* (1980*a*, *b*) investigated the supercritical regime, using visualization techniques to give an insight into the flow structure. In addition, Ruth *et al.* (1980*b*), Clever & Busse (1977) and Nagata & Busse (1983) have investigated the transition to secondary and tertiary instabilities.

In infinitely extended layers and for small Rayleigh numbers, it is possible to

define the basic state by means of a cubical velocity profile and a linear temperature distribution $T(z)$ (conduction regime). The stability problem becomes far more complex in containers with finite extension. The basic state becomes three-dimensional due to the deflection of the flow at the ends and the influence of the lateral walls. In a first systematic investigation of this subject, Hart (1971) studied the onset of instability of the basic flow in shallow boxes for the medium water. The influence of the lateral walls was still slightly noticeable at the chosen aspect ratio of 25:12:1 and 37:17:1. The onset of longitudinal rolls and transverse travelling waves, as well as the transition to turbulence, are summarized in a stability diagram. Comparable investigations for air were carried out by Linthorst, Schinkel & Hoogendoorn (1981), whereby the aspect ratio was additionally varied in the range $h_x:h_z = 7:1$ to $1:1$. Ozoe *et al.* (1977, 1983) have carried out theoretical and experimental investigations, mainly of long channels and containers with small aspect ratios, discussing in particular the three-dimensional flow structure. The calculation of particle path lines for selected parameters gives an insight into the complex spatial flow structure.

The basic state, defined in tilted boxes by a three-dimensional velocity and temperature field, must be known prior to carrying out stability investigations. Only in shallow boxes is it possible to approximate this basic state by means of an analytical approximate solution (Hart 1971). It is not possible to make an analytical description of the basic flow in all other cases, a fact which makes the stability calculation much more difficult. A suggestion for solving this problem is made within the framework of this paper. Critical Rayleigh numbers are calculated for two different Prandtl numbers as a function of the container inclination by iterative application of a finite-difference method and a Galerkin method. The extent to which the critical Rayleigh numbers, calculated under the assumption of linear stability theory, agree with the stability limits observed in the experiment is also investigated.

In closed boxes, there is an intricate superposition of basic flow and transverse or longitudinal convection rolls. The resultant three-dimensional flow is calculated by means of a finite-difference method. Finally, the transition to time-dependent solutions is experimentally investigated for two Prandtl numbers, and the results are summarized in stability diagrams.

The aim of this article is to investigate the influence of lateral walls on the problem of the Rayleigh–Bénard convection in horizontal and tilted boxes. The following questions are discussed:

(i) The influence of shear flows on the stability behaviour of cellular convection in tilted boxes. Here the novel aspect is the combination of a finite difference method and a Galerkin method in solving the stability problem theoretically. In this way the three-dimensional nature of the basic flow can be introduced in the stability calculations.

(ii) The influence of lateral walls and shear flows on the three-dimensional flow structure in the supercritical regime.

(iii) The transition to time-dependent solutions as a function of the angle of inclination and for three different Prandtl numbers, confirm the importance of nonlinear effects.

Special attention is paid to the interaction between experimental measuring techniques and the numerical approach to such a complex problem as thermal convection in closed boxes. Many aspects of the dynamics of nonlinear convection systems have been reported by other authors. Here, however, they are not reported

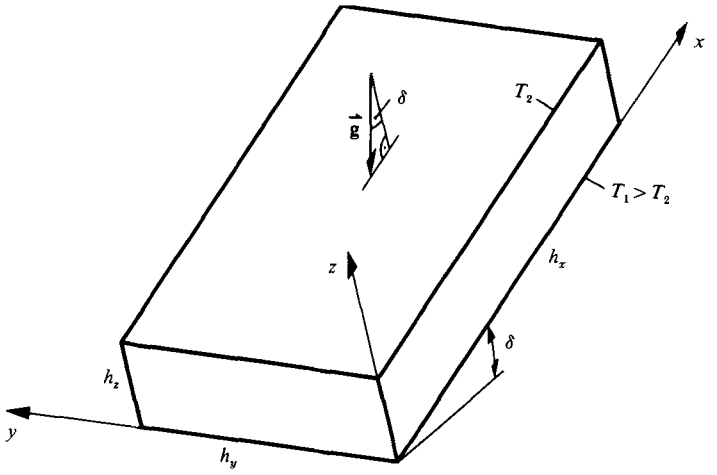

FIGURE 2. Principle sketch of the box and coordinate system.

because the connection between the temporal structure in the phase and spatial structure in the physical space, for three-dimensional convection flows in enclosed boxes, is not obvious; Oertel (1984).

2. Numerical simulation

2.1. *Basic equations*

In the case of the Rayleigh–Bénard convection of a horizontal layer heated from below, we can neglect the kinetic and potential energy and the dissipation in comparison with the internal energy. We assume a Newtonian medium and introduce the Boussinesq approximation. This means that all fluid properties, the viscosity ν, thermal conductivity λ and density ρ, are assumed to be constant. Only the temperature dependence of the density in the buoyancy term causing thermal convection is taken into account. This produces the following system of basic equations:

$$\left.\begin{aligned} \nabla\cdot\boldsymbol{v} &= 0, \\ \frac{1}{Pr}\left(\frac{\partial \boldsymbol{v}}{\partial t}+(\boldsymbol{v}\cdot\nabla)\,\boldsymbol{v}\right) &= -\nabla p+\Delta\boldsymbol{v}+Ra\,T\boldsymbol{k}, \\ \frac{\partial T}{\partial t}+(\boldsymbol{v}\cdot\nabla)T &= \Delta T, \\ Ra = \frac{\alpha\cdot g(T_1-T_2)\,h_z^3}{\nu\kappa}, \quad Pr &= \frac{\nu}{\kappa}. \end{aligned}\right\} \tag{2.1}$$

All quantities have been made dimensionless by scaling lengths with the height of the fluid layer h_z, velocities $\boldsymbol{v} = (u, v, w)$ with κ/h_z, where κ is the thermal diffusivity, time with h_z^2/κ, temperature with the temperature difference between the horizontal boundaries T_1-T_2 and pressure with $\rho\nu\kappa/h_z^2$. The Prandtl number Pr and the Rayleigh number Ra are the dimensionless parameters with the gravitational constant g, and α the thermal expansion coefficient. $\boldsymbol{k} = (1\cos\delta, 0, 1\sin\delta)$ denotes the unit vector. In the tilted box we limit ourselves to the case of a turn round the short container axis (see figure 2).

We perform a perturbation analysis of the heat conduction condition for calculating the onset of steady cellular convection in the case of horizontal fluid layers. At the onset of convection, the velocities and temperature derivatives are small, and the nonlinear terms of the momentum and energy equations can thus be neglected. This assumption enables us to produce the steady, linear basic equations for the disturbance variables $\boldsymbol{v}^*, T^*, p^*$.

$$\left.\begin{aligned} \boldsymbol{\nabla}\cdot\boldsymbol{v}^* &= 0, \\ 0 &= -\boldsymbol{\nabla}p^* + \Delta\boldsymbol{v}^* + Ra\,T^*\boldsymbol{k}(0°), \\ -w &= \Delta T^*. \end{aligned}\right\} \tag{2.2}$$

We assume the following boundary conditions for rigid and isothermal surfaces:

$$w = \frac{\partial w}{\partial z} = 0, \quad T^* = 0. \tag{2.3}$$

In a tilted box, there is always a basic flow present for each Rayleigh number other than 0; this basic flow is then eliminated using the following ansatz:

$$\left.\begin{aligned} \boldsymbol{v} &= \boldsymbol{v}_0 + \boldsymbol{v}^*, \\ T &= T_0 + T^*, \\ p &= p_0 + p^*, \\ T_0 &= \bar{T}(x,y,z) - \beta z \quad (\beta = 1). \end{aligned}\right\} \tag{2.4}$$

The index '0' indicates the basic state, which is separated as regards the temperature into one part caused by the basic flow ($\bar{T}(x,y,z)$) and one caused by heat conduction (βz). If we insert this formulation into the system of basic equations (2.1), we obtain the following set of equations for the basic solution and perturbation equations:

(*a*) Basic solution

$$\left.\begin{aligned} \boldsymbol{\nabla}\cdot\boldsymbol{v}_0 &= 0, \\ \frac{1}{Pr}\left(\frac{\partial\boldsymbol{v}_0}{\partial t} + (\boldsymbol{v}_0\cdot\boldsymbol{\nabla})\,\boldsymbol{v}_0\right) &= -\boldsymbol{\nabla}p_0 + \Delta\boldsymbol{v}_0 + Ra\,T_0\,\boldsymbol{k}, \\ \frac{\partial T_0}{\partial t} + (\boldsymbol{v}_0\cdot\boldsymbol{\nabla})\,T_0 &= \Delta T_0. \end{aligned}\right\} \tag{2.5}$$

(*b*) Perturbation equations

$$\left.\begin{aligned} \boldsymbol{\nabla}\cdot\boldsymbol{v}^* &= 0, \\ \frac{1}{Pr}\left[\frac{\partial\boldsymbol{v}^*}{\partial t} + (\boldsymbol{v}^*\cdot\boldsymbol{\nabla})\,\boldsymbol{v}_0 + (\boldsymbol{v}_0\cdot\boldsymbol{\nabla})\,\boldsymbol{v}^*\right] &= -\boldsymbol{\nabla}p^* + \Delta\boldsymbol{v}^* + Ra\,\boldsymbol{k}\,T^*, \\ \frac{\partial T^*}{\partial t} + (\boldsymbol{v}^*\cdot\boldsymbol{\nabla})\,\bar{T} + (\boldsymbol{v}_0\cdot\boldsymbol{\nabla})\,T^* - w &= \Delta T^*. \end{aligned}\right\} \tag{2.6}$$

Provided the main interest lies in the onset of cellular convection, the nonlinear terms $(\boldsymbol{v}^*\cdot\boldsymbol{\nabla})v^*$ and $(\boldsymbol{v}^*\cdot\boldsymbol{\nabla})T^*$ of the perturbation variables can be neglected. However, the equation still contains the coupling terms between basic solution and perturbation variables. This means that the basic flow's velocity and temperature field have to be known before the stability calculation can be carried out. Furthermore, the time derivatives $\partial v^*/\partial t$ and $\partial T^*/\partial t$ are considered to be equal to zero, when searching for steady solutions.

2.2. *Numerical methods*

The basic equations for the stationary and oscillatory convection in horizontal and inclined boxes have been solved by an explicit finite-difference method. The papers by Lipps (1976) and Oertel (1979) provide the basis of the three-dimensional difference method employed. The explicit Dufort–Frankel scheme described in the book by Richtmyer & Morton (1967) with second-order truncation error is applied. The nonlinear terms in the momentum and energy equations are represented by a difference scheme proposed by Piacsek & Williams (1970). A Poisson equation for the pressure is solved numerically, using the procedure described by Roache (1972). If the momentum equations are differentiated, the sum of these equations leads to the following pressure equation:

$$\Delta p = 2\left(\frac{\partial u}{\partial x}\frac{\partial v}{\partial y}+\frac{\partial u}{\partial x}\frac{\partial w}{\partial z}+\frac{\partial v}{\partial y}\frac{\partial w}{\partial z}-\frac{\partial v}{\partial x}\frac{\partial u}{\partial y}-\frac{\partial w}{\partial x}\frac{\partial u}{\partial z}-\frac{\partial w}{\partial y}\frac{\partial v}{\partial z}\right)+Ra\left(\frac{\partial T}{\partial x}\sin\delta+\frac{\partial T}{\partial z}\cos\delta\right). \tag{2.7}$$

The pressure field at every timestep is calculated implicitly by means of a method of cyclic reduction described by Schumann (1976).

The calculation method starts with the eigenfunctions of the linear stability problem, as described in §2.1, applying the Galerkin method of Kessler, Dallmann & Oertel (1983). This procedure corresponds to the experiment, since the cellular convection arises from a steady state of periodic velocity and temperature distribution in the x- and y-directions. The calculation method was optimized as regards the sizes of the grid intervals, and works with automatically controlled length of time intervals.

Particular attention was paid to ensuring the correct timestep in the numerical simulation calculation. Fundamental investigations by Kirchartz *et al.* (1982) have shown, by comparison with the experimental time-based increase of the flow amplitude of convective instabilities, that the applied numerical method is sufficiently accurate. This is a basic presupposition for the numerical calculation of time-dependent convection flows.

In the regime of supercritical cellular convection, the calculations were carried out for two different container geometries. The intermediate aspect ratio $h_x:h_y:h_z = 10:4:1$ is selected to obtain a well-defined flow pattern, which in the central part of the container can be assumed as a nearly two-dimensional flow. In the neighbourhood of the lateral walls, however, three-dimensional effects will be dominant and will, as shown later, significantly influence the stability mechanisms. For the time-consuming simulation of the oscillatory convection, a second smaller aspect ratio box of $h_x:h_y:h_z = 4:2:1$ is selected. The number of grid points differed accordingly, between $81\times33\times17$ for the larger and $41\times21\times17$ for the smaller box.

The majority of the three-dimensional numerical calculations were carried out on the vector computer CYBER 205 of the University of Karlsruhe, using a nearly full-vectorized computer code. For a domain of $41\times21\times17$ grid points a c.p.u.-time of 110 milliseconds per timestep is needed. The steady state, for not too high Rayleigh numbers ($Ra < 10000$), is reached after 300–600 timesteps.

The finite-difference method is used to calculate the three-dimensional flow structure in the supercritical regime. A Galerkin method, briefly described below, is used to solve the linear stability problems for both the horizontal and the tilted box. In contrast to figure 2, the origin of the coordinates is now placed at the centre of the box.

The unknown functions for the perturbation variables velocity $\boldsymbol{v}^*$, temperature T^* and pressure p^* are expanded into complete sets of functions $\boldsymbol{F}_j, G_j$ and H_j, a_j, b_j and c_j being the expansion coefficients yet to be determined.

$$\boldsymbol{v}^* = \sum_{j=1}^{N} a_j \boldsymbol{F}_j(x,y,z), \quad T^* = \sum_{j=1}^{M} b_j G_j(x,y,z), \quad p^* = \sum_{j=1}^{L} c_j H_j(x,y,z). \tag{2.8}$$

The trial functions are chosen in such a manner as to fulfil the boundary conditions and the continuity equation while eliminating the pressure term in the momentum equation.

If we introduce the ansatz (2.8) into the linear momentum and energy equations (2.6), then, as we can only expect an approximate solution, the sum of all terms will be $\epsilon \neq 0$. We thus obtain the two error functions, $\boldsymbol{\varepsilon}_1$ for the momentum equation and ϵ_2 for the energy equation.

$$\left.\begin{aligned} \sum_{j=1}^{N} a_j \Delta \boldsymbol{F}_j + Ra\,\boldsymbol{k} \sum_{j=1}^{N} b_j G_j - \sum_{j=1}^{L} c_j \nabla H_j - \frac{1}{Pr} \sum_{j=1}^{N} a_j (\boldsymbol{F}_j \cdot \nabla)\, \boldsymbol{v}_0 - \frac{1}{Pr} \sum_{j=1}^{N} a_j (\boldsymbol{v}_0 \cdot \nabla)\, \boldsymbol{F}_j = \boldsymbol{\varepsilon}_1, \\ \sum_{j=1}^{N} a_j (\boldsymbol{F}_j \cdot \nabla) \bar{T} + \sum_{j=1}^{M} b_j (\boldsymbol{v}_0 \cdot \nabla) G_j - \sum_{j=1}^{M} a_j \boldsymbol{e}_z \boldsymbol{F}_j - \sum_{j=1}^{M} b_j \Delta G_j = \epsilon_2. \end{aligned}\right\} \tag{2.9}$$

The Galerkin method requires that $\boldsymbol{\varepsilon}_1$ be orthogonal to each of the N trial functions $\boldsymbol{F}_k$, and that ϵ_2 be orthogonal to the corresponding trial functions G_k. For this purpose, the scalar product between error function and trial function is made, and the equations are integrated over the considered volume. The result is a system of $N+M$ homogeneous, linear algebraic equations for the unknown coefficients a_j and b_j. By applying the continuity equation and Gauss theorem, it can be shown that the pressure term is:

$$\int \sum_{j=1}^{L} c_j \nabla H_j \boldsymbol{F}_k \, \mathrm{d}V = 0. \tag{2.10}$$

The definitive Galerkin equations in matrix notation are:

$$\boldsymbol{A}^{NN} \boldsymbol{a} + Ra\, \boldsymbol{B}^{NM} \boldsymbol{b} = 0, \quad \boldsymbol{C}^{MN} \boldsymbol{a} + \boldsymbol{D}^{MM} \boldsymbol{b} = 0, \tag{2.11}$$

$a = (a_1, \ldots, a_N)$ and $b = (b_1, \ldots, b_M)$ are the vectors of the unknown expansion coefficients. The elements of the matrices $\boldsymbol{A}^{NN}$ $\boldsymbol{B}^{NM}$ $\boldsymbol{C}^{MN}$ and $\boldsymbol{D}^{MM}$ are made up of the following terms:

$$\left.\begin{aligned} A_{kj} &= \int \boldsymbol{F}_k \Delta \boldsymbol{F}_j \, \mathrm{d}V - \frac{1}{Pr} \int \boldsymbol{F}_k (\boldsymbol{F}_j \cdot \nabla)\, \boldsymbol{v}_0 \, \mathrm{d}V - \frac{1}{Pr} \int (\boldsymbol{v}_0 \cdot \nabla)\, \boldsymbol{F}_j \boldsymbol{F}_k \, \mathrm{d}V, \\ B_{kj} &= \int \boldsymbol{k} \boldsymbol{F}_k G_j \, \mathrm{d}V, \\ C_{kj} &= \int G_k (\boldsymbol{F}_j \cdot \nabla) \bar{T} \, \mathrm{d}V - \int \boldsymbol{e}_z \boldsymbol{F}_j G_k \, \mathrm{d}V, \\ D_{kj} &= \int G_k (\boldsymbol{v}_0 \cdot \nabla) G_j \, \mathrm{d}V - \int G_k \Delta G_j \, \mathrm{d}V. \end{aligned}\right\} \tag{2.12}$$

The Rayleigh number is the parameter of this system of equations. When the determinant of the coefficient matrix vanishes, the system of equations has a non-

trivial solution. The determinant's zero is approximated by means of quadratic interpolation. Thus, the smallest Rayleigh number found represents the critical value required for the onset of cellular convection.

By introducing the critical Rayleigh number obtained into the Galerkin equations, and by employing Gauss elimination procedure, it is possible, for instance, to determine the vectors $\boldsymbol{a}$ and $\boldsymbol{b}$ up to a constant factor. Once introduced in the relations (2.8), we obtain the eigenfunctions for velocity and temperature. These are then chosen as the initial distribution for application of the difference method to supercritical flow conditions.

The successful application of the Galerkin method depends on the appropriate selection of the trial functions for velocity and temperature. For the velocity, we use the following ansatz for a non-divergent vector field:

Motion in the (x, z)-plane: basic flow and transverse rolls

$$\boldsymbol{F}_j = \boldsymbol{\nabla} \times (\psi_j \cdot \boldsymbol{e}_y) = \left(-\frac{\partial \psi_j}{\partial z},\ 0,\ \frac{\partial \psi_j}{\partial x} \right). \tag{2.13}$$

Motion in the (y, z)-plane: longitudinal rolls

$$\boldsymbol{F}_j = \boldsymbol{\nabla} \times (\phi_j \cdot \boldsymbol{e}_x) = \left(0, \frac{\partial \phi_j}{\partial z}, -\frac{\partial \phi_j}{\partial y} \right), \tag{2.14}$$

ψ_j and ϕ_j are three-dimensional scalar functions, separated according to the three spatial coordinates.

$$\psi_j = f_{p_j}(x)\, g_{q_j}(y)\, h_{r_j}(z), \quad \phi_j = g_{p_j}(x) f_{q_j}(y)\, h_{r_j}(z). \tag{2.15}$$

The integer indices p_j, q_j and r_j are varied independently of each other. The functions f and h, as well as their derivatives, must be zero at the walls in order to fulfil the boundary conditions. These requirements fulfil the 'Beam–Functions' described in the paper by Harris & Reid (1958).

Even function

$$C_m(x) = \frac{\cos h(\lambda_m x)}{\cos h(\frac{1}{2}\lambda_m)} - \frac{\cos(\lambda_m x)}{\cos(\frac{1}{2}\lambda_m)}. \tag{2.16}$$

Odd function

$$S_m(x) = \frac{\sin h(\mu_m x)}{\sin h(\frac{1}{2}\mu_m)} - \frac{\sin(\mu_m x)}{\sin(\frac{1}{2}\mu_m)}, \tag{2.17}$$

λ_m and μ_m are chosen in such a manner as to fulfil the above requirements. For reasons of symmetry, when applying the Galerkin method, we locate the origin of the system of coordinates in the middle of the box (contrary to figure 2):

Trigonometrical functions are sufficient for the temperature expansion, since only the perturbation temperature at the walls has to vanish.

All possible combinations of even and odd function systems must be considered in the formation of the matrices (2.12), as must the formulations for the basic solution, which are likewise made up of several function systems. Solving the system of equations thus created requires a great deal of effort. Therefore, we only consider those function systems which are physically reasonable, or those which have an influence on the eigenvalue. This selection was carried out with the aid of test calculations.

The following function systems are used:
Basic flow:

$$\left.\begin{aligned}
&\psi_j = C_{p_j}\left(\frac{x}{h_x}\right)\cos\left((2q_j-1)\frac{\pi y}{h_y}\right)C_{r_j}(z) \quad (p_j = 1,\ldots,9;\ q_j = 1;\ r_j = 1),\\
&G_j^{(1)} = \sin\left(2p_j\pi\frac{x}{h_x}\right)\cos\left((2q_j-1)\pi\frac{y}{h_y}\right)\cos\left((2r_j-1)\pi z\right)\\
&\qquad\qquad (p_j = 1,\ldots,9;\ q_j = 1;\ r_j = 1),\\
&G_j^{(2)} = \cos\left((2p_j-1)\pi\frac{x}{h_x}\right)\cos\left((2q_j-1)\pi\frac{y}{h_y}\right)\sin\left(2r_j\pi z\right)\\
&\qquad\qquad (p_j = 1,2,3;\ q_j = 1;\ r_j = 1).
\end{aligned}\right\} \tag{2.18}$$

Transverse rolls (odd number of rolls)

$$\left.\begin{aligned}
&\psi_j^{(1)} = C_{p_j}\left(\frac{x}{h_x}\right)\cos\left((2q_j-1)\pi\frac{y}{h_y}\right)C_{r_j}(z) \quad (p_j = 1,\ldots,10;\ q_j = 1;\ r_j = 1,2),\\
&\psi_j^{(2)} = S_{p_j}\left(\frac{x}{h_x}\right)\cos\left((2q_j-1)\pi\frac{y}{h_y}\right)S_{r_j}(z) \quad (p_j = 2,\ldots,9;\ q_j = 1;\ r_j = 1),\\
&G_j^{(1)} = \sin\left(2p_j\pi\frac{x}{h_x}\right)\cos\left((2q_j-1)\pi\frac{y}{h_y}\right)\cos\left((2r_j-1)\pi z\right)\\
&\qquad\qquad (p_j = 1,\ldots,10;\ q_j = 1;\ r_j = 1,2),\\
&G_j^{(2)} = \cos\left((2p_j-1)\pi\frac{x}{h_x}\right)\cos\left((2q_j-1)\pi\frac{y}{h_y}\right)\sin\left(2r_j\pi z\right)\\
&\qquad\qquad (p_j = 2,\ldots,9;\ q_j = 1;\ r_j = 1).
\end{aligned}\right\} \tag{2.19}$$

Longitudinal rolls (even number of rolls)

$$\left.\begin{aligned}
&\phi_j^{(1)} = \cos\left((2p_j-1)\pi\frac{x}{h_x}\right)S_{q_j}\left(\frac{y}{h_y}\right)C_{r_j}(z)\\
&\qquad\qquad (p_j = 1,2,3;\ q_j = 1,\ldots,4;\ r_j = 1,2,3),\\
&\phi_j^{(4)} = \sin\left(2p_i\pi\frac{x}{h_x}\right)S_{q_j}\left(\frac{y}{h_y}\right)S_{r_j}(z) \quad (p_j = 1,2,3;\ q_j = 1,\ldots,4;\ r_j = 1,2,3),\\
&G_j^{(1)} = \cos\left((2p_j-1)\pi\frac{x}{h_x}\right)\cos\left((2q_j-1)\pi\frac{y}{h_y}\right)\cos\left((2r_j-1)\pi z\right)\\
&\qquad\qquad (p_j = 1,2,3;\ q_j = 1,\ldots,4;\ r_j = 1,2,3),\\
&G_j^{(2)} = \cos\left((2p_j-1)\pi\frac{x}{h_x}\right)\cos\left((2q_j-1)\pi\frac{y}{h_y}\right)\sin\left(2r_j\pi z\right)\\
&\qquad\qquad (p_j = 1,2,3;\ q_j = 1,\ldots,4;\ r_j = 1,2,3).
\end{aligned}\right\} \tag{2.20}$$

The basic state at the critical point must be known in order to calculate the onset of cellular convection in the tilted box using a Galerkin method. This basic state, however, is itself a function of the Rayleigh number sought, and cannot be analytically specified in the case of closed containers. To solve this problem, we

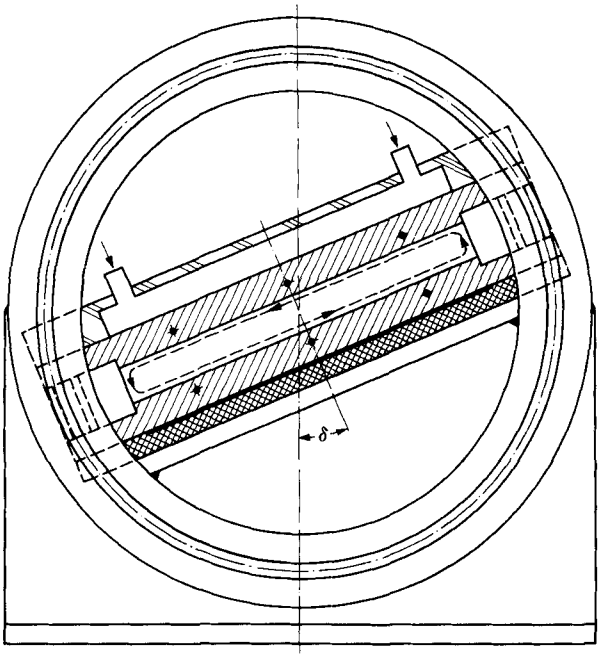

FIGURE 3. Cross-section of the convective apparatus.

propose iterative application of a combined finite-difference method and a Galerkin method.

The eigenvalue calculation at a given angle of inclination can be described as follows: first, the basic flow is calculated for an estimated Rayleigh number with the aid of a finite-difference method. The first approximation for the critical Rayleigh number is based on the known experimental results. Moreover, starting from $\delta = 0°$, the stability curve is calculated in small angle steps, so that we can always be guided by a neighbouring eigenvalue. The velocity and temperature field of the basic solution calculated in discrete points is represented in the form of the function systems (2.18), using the least squares method. The calculated coefficients $a_j\,(j = 1, \ldots, 9)$ and $b_j\,(j = 1, \ldots, 12)$ required for the basic solution are introduced in the coupling elements between basic flow and cellular convection of the Galerkin method. The second approximation for the critical Rayleigh number is obtained as a result of the eigenvalue calculation. The iteration procedure is interrupted when a given approximation level for the calculation of the critical Rayleigh number is reached. The number of iterations should be kept within limits, as the method is very time-consuming. If the first approximation for the Rayleigh number is selected carefully, its value can be determined to within less than 1% after only 3 iterations.

3. Experiments

The experiments serve to test the physical models and permit a quantitative study of possible steady and time-dependent flow patterns appearing as a function of Rayleigh and Prandtl numbers, angle of inclination and aspect ratio.

Figure 3 shows the cross-section of the test cell. It consists of two horizontal,

perfectly-conducting copper plates. The lower plate is electrically heated by a heater foil, while the upper is kept at a constant temperature by means of a thermostat-controlled water bath. Using thermistors, the temperature difference between the two copper plates can be measured to within ± 0.005 K. Each plate temperature can be adjusted to within ± 0.01 K (heating) and ± 0.02 K (cooling) and kept constant over a long period. The mean temperature in the test cell is adjusted to room temperature to minimize the heat exchange between test cell and environment. Only in the case of the sensitive measurements with nitrogen as test fluid was the test cell vacuum-isolated. The height of the test cell was chosen in such a way, considering the test fluid to be used and the Rayleigh number regime to be investigated, as to fulfil the assumptions of the Boussinesq approximation, meaning that the variation of the relevant fluid properties over the height of the test cell should not exceed 10%.

The glass borders were made of quartz or plate-glass panes to adapt to optical measuring techniques. These glass borders, together with the test fluid used, determine the thermal boundary conditions. The thermal boundary condition can be classified using the definition of a wall admittance parameter C, proposed by Catton (1978) ($C = \lambda_{\mathrm{fl}} \cdot h_z / \lambda_{\mathrm{w}} \cdot d_{\mathrm{w}}$ with λ_{fl} and λ_{w} the heat conductivities of the fluid and the wall respectively and d_{w} the thickness of the lateral walls.) In our experiments the following values for C exists: C (air/glass) = 0.014, C (silicone oil/glass) = 0.083 and C (water/glass) = 0.342. These values of C indicate that the assumption of perfectly conducting sidewalls is fulfilled in the experiments especially for the test fluids air and silicone oil and approximately also for water.

Several optical measuring techniques are used to investigate the various steady and time-dependent convection processes. These allow contactless and thus perturbation-free investigation of flows in transparent media. This is a necessary precondition for quantitative investigation of absolutely unstable stability problems. Thus, not only flow visualizations are possible, but also quantitative statements about density and velocity fields.

Interferometrical methods are useful for studying convective flows with typical density and temperature distributions. The differential interferometer used in this work proved extremely advantageous in the above investigations. Not only is it insensitive to vibrations and easy to adjust, but its sensitivity can be adapted to the various test fluids by simply exchanging the beam splitting components.

Figure 4(*a*) shows the principal set-up of the differential interferometer used. The light source Q delivers monochromatic light, which is polarized at 45° (Polarizer P_1) and meets on the Wollaston prism W_1. Each light beam is here split up into two beams polarized in perpendicular directions. These cross the test region M with a constant beam separation e. This beam separation e determines the sensitivity of the interferometer and can be modified by choosing different Wollaston prisms. After recombination in prism W_2, their 45° components are finally brought to interference after passing the polarizer's plane P_2. The objective O produces a picture of the test cell which is focused on the film screen F. With sufficiently large density gradients, a system of interference fringes is produced that permits quantitative evaluation of the integral density distribution.

Greater sensitivity, as required, for instance, for measurements in gas, is obtained with a special laser-differential interferometer (figure 4*b*) which differs from the total-field differential interferometer in two design features. A laser L (HeNe Laser, 5mW) is used as light source, its light beam being focused on the measuring plane M. The interference signal is measured with a PIN diode (PI). This allows measurement of

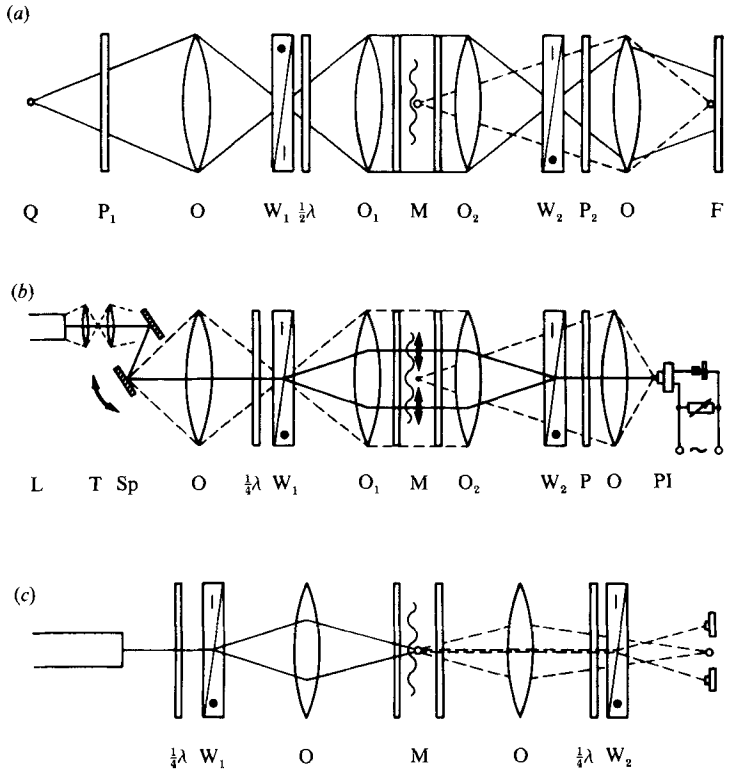

FIGURE 4. Optical measuring techniques. (*a*) $\frac{1}{2}\lambda$-compensated differential interferometer. (*b*) Laser-differential interferometer with scanning mirror. (*c*) Laser-Doppler anemometer.

the phase shift of the two beams, induced by the integral density gradients, up to fractions of the light wavelength λ. A scanning mirror Sp enables the interferometer beams to be moved relative to the measuring object, making the determination of density profiles possible.

We use the laser-differential interferometer in three different cases:

(*a*) Onset of steady convection in nitrogen. Very small deviations of the heat conduction profile must be registered in this case.

(*b*) Transition from steady to time-dependent cellular convection. The onset of periodic density variations is registered by means of a fixed interferometer beam. This method, however, cannot be applied when analysing oscillation frequencies. As the flow becomes more and more three-dimensional, it is impossible for the integral density signal to give information about the change of local flow properties. Therefore, the periodic temperature change at a specific place is measured using thermocouples.

(*c*) The third application deviates from its normal use. After removing the Wollaston prism W_1, the set-up presented in figure 4(*b*) can be used as a light cut method. A light sheet is formed in the measuring area by moving the scanning mirror at a sufficiently high frequency. Then, by adding small particles to the fluid, it is possible, using long time exposures, to produce streak-line photographs which permit the flow to be visualized in a simple manner.

Further details on the optical set-up and operation of differential interferometers, as

well as quantitative evaluation of interferograms, can be found in the publications by Kirchartz (1980), Oertel (1961), Oertel & Bühler (1978) and Oertel & Oertel Jr (1988).

A special type of laser-Doppler anemometer described by Bossel, Hiller & Meier (1972) is used to measure local velocity. The very small velocities in convection flows cause the Doppler frequencies to lie typically in the range of 10 Hz to 10 kHz, with which a very low noise ratio is associated. The set-up shown in figure 4(*c*) solves this problem by means of optical signal filtering. A Wollaston prism serves as beam splitting component. The two beams polarized perpendicularly cross each other in the measuring volume. By observing the intersection of the laser beams through a combination of $\frac{1}{4}\lambda$ plate and Wollaston prism W_2, it is possible to detect two $\frac{1}{2}\lambda$ shifted systems of interference fringes. Therefore, two complementary scattered light signals can be measured on both light detectors. If the two signals are subtracted, the amplitude of the Doppler signal will double, and the remaining scattered light elements and light fluctuation will virtually disappear. We were able to measure velocities down to 5.10^{-6} m/s with this set-up.

4. Onset of cellular convection

First of all we will discuss the onset of cellular convection in horizontal boxes. Only in the case $\delta = 0°$ does there exist a basic state of pure heat conduction, meaning without any motion, that can be described analytically by the linear heat conduction profile. In figure 5 the calculated critical Rayleigh numbers are plotted against the normalized length h_x/h_z ($h_y/h_z = \text{const} = 4$). The influence of increasing critical Rayleigh numbers with decreasing aspect ratio is known from earlier calculations of Catton (1970) and Davis (1967). Over a wide range our values are somewhat smaller than the corresponding results published by these two authors. One reason may be the higher number of trial functions used in our stability analysis. In any case the results of figure 5 agree very well with the measured critical Rayleigh numbers for some selected aspect ratios, among them the two geometries discussed in the present paper.

In tilted boxes however there exists, below a supercritical Rayleigh number, a weak basic flow which must be considered as a three-dimensional flow in the case of closed boxes; the basic state can no longer be described analytically. Therefore the onset of steady cellular convection was calculated following the iterative application of a combined finite-difference method and a Galerkin method, as described in §2.2. The results of these eigenvalue calculations are shown in figure 6 for a specified container geometry and two different Prandtl numbers. The critical Rayleigh number is plotted as a function of the angle of inclination, at which the basic state turns unstable. Basically, it is the straight rolls that superimpose on the basic flow, whereby we have to distinguish between two types of rolls: transverse rolls lie with their axes perpendicular to the basic flow and, as a result of the container's chosen turning axis, are identical with the rolls parallel to the shorter side of the box (solution for the case $\delta = 0°$). Longitudinal rolls orient themselves with their axes along the basic flow. In horizontal boxes, the rolls parallel to the shorter side of the box seem to be the preferred solution, since they have the smallest eigenvalue (1817 versus 1883 for the rolls parallel to the longer side of the box).

In the case of a weak basic flow ($\delta \leqslant 12°$), the transverse rolls will retain the smaller eigenvalue, then constituting the preferred physical solution. At larger angles of inclination ($\delta > 12°$), the increasing shear effect of the basic flow forces the transverse

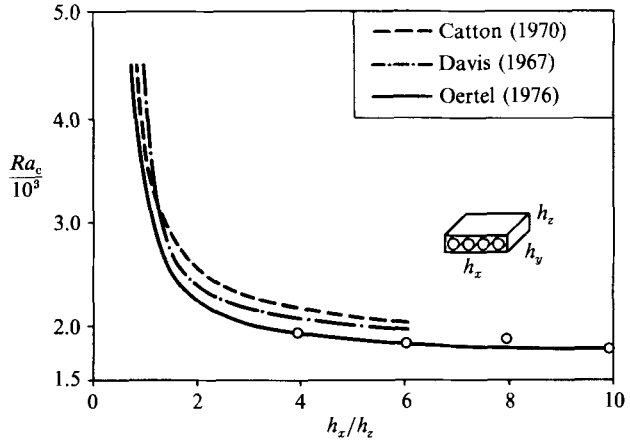

FIGURE 5. Critical Rayleigh number as a function of the aspect ratio h_x/h_y with $h_y/h_z = \text{const.}$ ——, theory; ○, experiment.

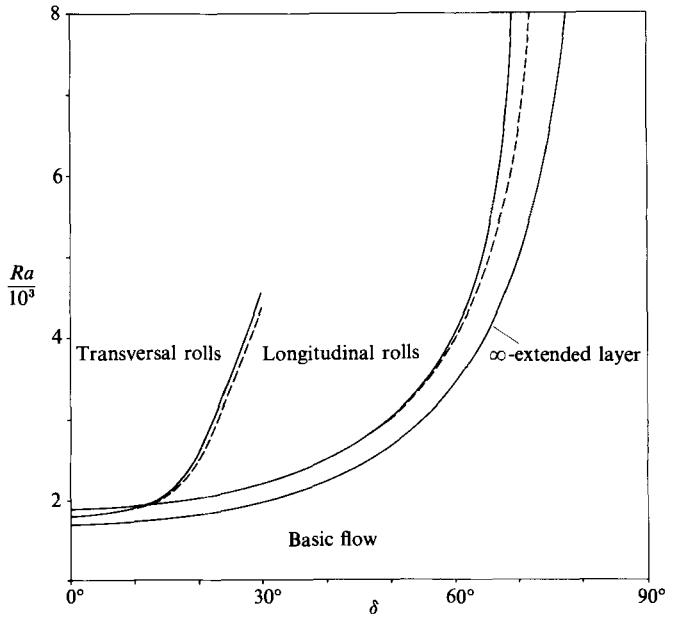

FIGURE 6. Critical Rayleigh number in tilted boxes. Linear theory. Aspect ratio = 10:4:1; – – –, $Pr = 0.71$; ——, $Pr = 7.0$.

rolls to reorient towards the longitudinal rolls, whereby the critical Rayleigh number increases progressively with increasing angle of inclination (the fact that a definite amount of shear is required to convert transverse rolls to longitudinal rolls when sidewalls are present is also known from other flow configurations e.g. Poiseuille flow heated from below, see Platten & Legros 1984). As a comparison, we present the value for infinitely extended fluid layers, where the critical Rayleigh number can be calculated by the simple relationship $Ra_c = 1708/\cos\delta$.

Consequently, the value of the critical Rayleigh number in the tilted box is determined by three factors:

(i) Cellular convection is caused by the part $g\cos\delta$ of the gravitational acceleration, and so the limit case $\delta = 90°$ constitutes an asymptotic value.

	Ra_c
Infinitely extended fluid layer	4994
Only sidewalls considered	5505
Considering the basic flow	9401

TABLE 1. Critical Rayleigh numbers, $\delta = 70°$, $Pr = 7.0$

(ii) The stabilizing influence of the lateral walls increases the Rayleigh number by a constant factor ($k = 1883/1708$ for longitudinal rolls and an aspect ratio of 10:4:1).

(iii) Finally, the basic flow has an inhibiting influence on the onset of cellular convection, this influence strongly increasing at larger angles. This is clarified by the example $\delta = 70°$ in table 1. In closed boxes, the basic flow already transports heat by convection between the isothermal walls, thus deferring the onset of cellular motion. Because of the lower Prandtl number, the convective transport of the basic flow is less marked in nitrogen than in water. The stabilizing influence on the development of cellular convection is correspondingly smaller. The extent to which the results of the linear stability theory agree with the experimental observations will be discussed in §7.1.

As the first result of this paper we will emphasize that the stability analysis of cellular convection, under the influence of shear flows, is quite sensitive to the introduction of the correct basic state in the calculation process.

5. Steady Rayleigh–Bénard convection

At the beginning of the next section we will return to the case of cellular convection in horizontal containers of intermediate aspect ratio and will discuss some important features of the three-dimensional effects in the supercritical regime. The finite-difference-method test calculations have shown, that the numerical solutions may depend on the initial flow field distribution chosen at the beginning of the calculation; here the experiment is a guide for the calculation. We chose the eigenfunctions of the critical Rayleigh number determined with the aid of the linear stability theory as initial distribution for the velocity and temperature fields. The amplitude of the initial distribution is fixed at approximately 1 % of the value of the stationary final solution. The stationary solution is first calculated for a slightly supercritical Rayleigh number. From this result, it is then possible to determine further solutions by slowly (quasi-stationary) increasing the Rayleigh number.

Figure 7 presents the result of a calculation for $Pr \gg 1$. The distribution of the vertical velocity component on the horizontal midlayer ($z/h_z = 0.5$) is shown. Ten convection rolls with their axes parallel to the shorter side of the container were formed. The chosen geometry permits the assumption of a two-dimensional flow at the centre of the measuring cell. In actual fact, however, noticeable velocity components, caused by buoyancy and inertial forces, develop parallel to the rolls' axes, so that the assumption of a two-dimensional flow can only be partially fulfilled. The v component of the velocity vector already reaches 15 % of w_{max} at the relatively low Rayleigh number $Ra = 4000$. The no-slip condition at the border influences the flow field over the lengthscale h_z, and is particularly marked at the corners. The

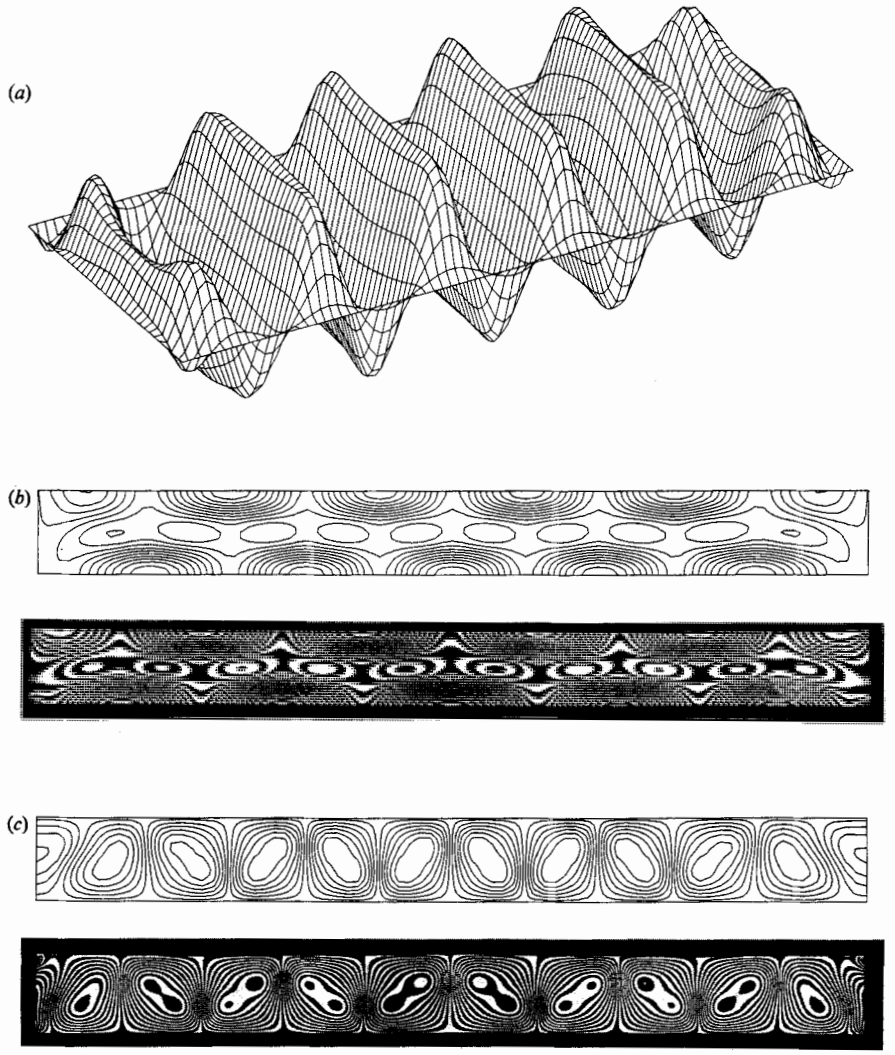

FIGURE 7. Steady cellular convection. $Ra = 4000$, $Pr \gg 1$, aspect ratio $h_x : h_y : h_z = 10:4:1$. (*a*) Distribution of the vertical velocity component w in the horizontal midlayer ($z/h_z = 0.5$). (*b*) Differential interferogram with vertical beam separation (lines of equal vertical density gradients). Test fluid: silicone oil, $Pr = 1780$. (*c*) Differential interferogram with horizontal beam separation (lines of equal horizontal density gradients).

calculated velocity amplitude and the Nusselt number approximately agree with two-dimensional calculation results.

Figure 7(*b*) presents a comparison of experimentally obtained differential interferograms and interferograms reconstructed from numerical solutions. The interference fringes represent lines of constant vertical or horizontal density gradients. Comparison of the figures confirms that the numerical solution method, in the main, also correctly describes the amplitude function and the structure of steady cellular convection.

Figure 8 presents comparable results for a Prandtl number of $Pr = 0.71$. In agreement with experimental observations, a solution with 9 convection rolls was

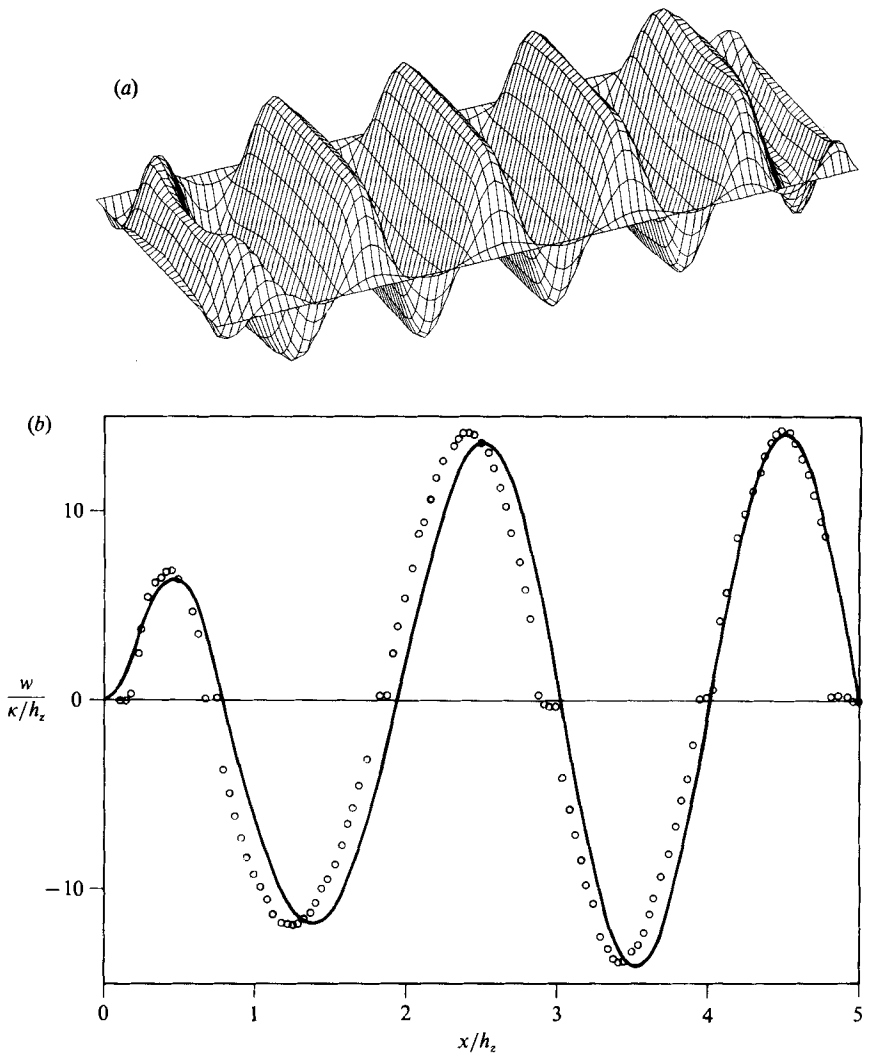

FIGURE 8. Steady cellular convection in nitrogen/air. $Ra = 4000$, $Pr = 0.71$, aspect ratio 10:4:1. (*a*) Distribution of the vertical velocity component w in the horizontal midlayer ($z/h_z = 0.5$). (*b*) Measured and calculated velocity profile $w(x, y = 2, z = 0.5)$. ——, numerical simulation; ○, measured values (LDA).

calculated for $Ra = 4000$. Here, too, a comparison of a measured velocity profile (see figure 7*b*) shows that the flow amplitude of the single rolls is correctly reproduced. The amplitude function is somewhat shifted by the varying size of the border roll. One reason for this may be that the perfectly conducting thermal boundary condition is only partially fulfilled in the experiment.

Only the modification of the wavelength, which develops in discrete steps in the container as a result of the finite number of rolls, cannot be satisfactorily described by the numerical simulation. The initial distribution given by the eigenfunctions essentially determines the number of convection rolls calculated numerically. The number of cells corresponding to a given Rayleigh or Prandtl number must, therefore, be included as a parameter in the calculation. But a modification in the number of cells does not take place as in the experimentally observed transition

Rayleigh numbers. One reason for this result may be the rather short computing time. In fact, experiments in air showed that a modification in the number of cells is reached through total reorientation of the flow field. This process runs over a time interval of several minutes in the selected measuring cell with $h_x = 15$ mm. However, even with the CYBER 205 vector computer, more than 30 hours CPU time would be required numerically to simulate a real time of, say, 5 minutes. This leads to the conclusion that the modification in the number of cells occurs in timescales which are an order of magnitude larger than the building-up time for a quasi-stationary solution. The numerical model calculation cannot reproduce this process with justifiable expenditure.

The experiments are unequivocal. With increasing Rayleigh number, they show a decrease in the number of cells N in convection boxes, and thus an increase in the wavelength of the convection cells. The wavelength was determined by means of interferometrical measurements, or by the velocity profiles obtained through the LDA. Figure 9(*a*) shows a series of interferograms for the test fluid water ($Pr = 7.0$). The rolls can easily be identified with the aid of the interference fringes. Beginning with 10 rolls for slightly supercritical Rayleigh numbers, the number of cells will decrease to 7 before oscillatory convection sets in ($Ra_{\mathrm{osc}} = 42000$).

As a summary of all experimental investigations, figure 9(*b*, *c*) shows, by the example of two different aspect ratios, the number of cells N or the wavenumber a as a function of the Rayleigh and Prandtl numbers. Smaller box geometries have a stabilizing effect on the transition process. The discrete wavelength increase takes place with media having larger Prandtl numbers at larger Rayleigh numbers. This is in full agreement with the theoretical results in infinitely extended horizontal layers. Clever & Busse (1978) were able to show that three-dimensional perturbations can lead to the so-called 'skewed varicose instabilities', with a greater effective wavelength.

The transition to turbulence is described in §6. In order to keep the calculation time within limits, these investigations were carried out using as an example a box with an aspect ratio of 4:2:1. Since time-dependent solutions are largely determined by three-dimensional effects, we shall use this example to discuss once again a number of characteristics of three-dimensional steady convection. A detailed discussion of three-dimensional convection in boxes can be found in the papers of Oertel (1980) and Kessler (1987). The main points, however, are summarized later on in this article. Three longitudinal convection rolls are found in the 4:2:1 box at the onset of oscillatory convection (critical Rayleigh number $Ra = 34000$).

Figure 10(*a*) shows a streak-line photograph of a cross-section through the convection rolls, and a numerically reconstructed streak-line picture obtained by the integration of particle paths from the calculated velocity field. At first glance this picture gives the impression of an even flow. In fact, analysis of the particle paths in the middle cross-section shows that these begin at the centre of the middle cell and end in the corner vortices. An idea of the flow field's three-dimensionality can be gained from the discussion of the velocity field's v component (velocity component parallel to the axis of the cell). These velocity profiles for the areas of upward and downward motion, as well as those for the cell's middle, are plotted in figure 10(*b*). The lateral walls influence the development of three-dimensional flows in two ways. First, inertial forces induce an axial flow, whereby pressure gradients make the medium at the outer part of the roll flow towards the wall, and back in the vicinity of the roll's axis (rotating flow over resting ground). Buoyancy forces close to the wall support this effect in the case of perfectly conducting lateral walls. Figure 10(*c*)

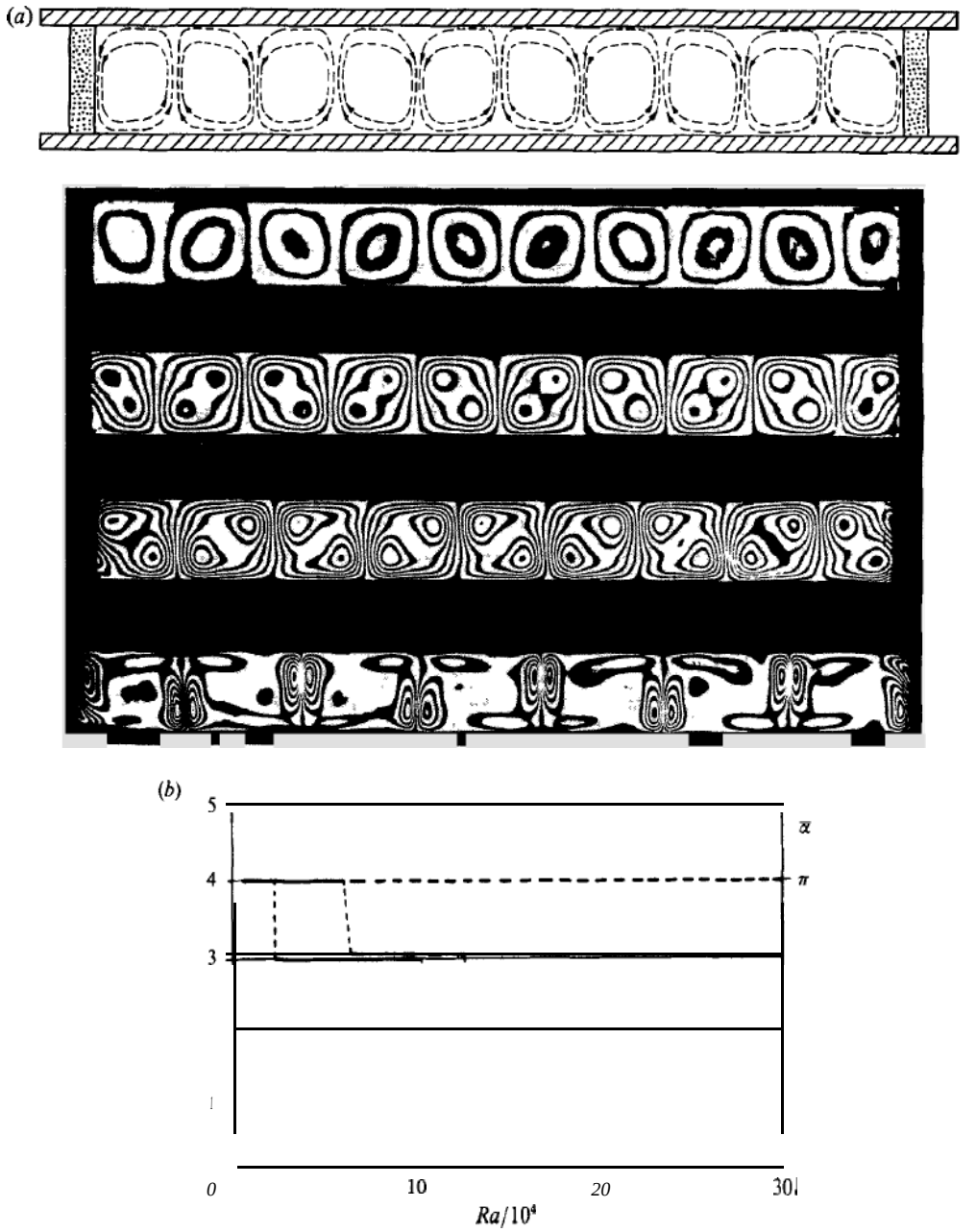

FIGURE 9(a, b). For caption see facing page.

shows plots of isotherms for a convection roll in the upward zone, in the downward zone and also in the middle of the cell. The isotherms are clearly shifted towards the border due to convective energy transport. However, local horizontal temperature gradients develop as the temperature at the wall is kept constant by the effective boundary condition. This causes an additional convective motion which is superimposed on the cellular convection in the direction of the arrows. Since the convection rolls represent motion in the (x, z)-plane, the v component of the velocity

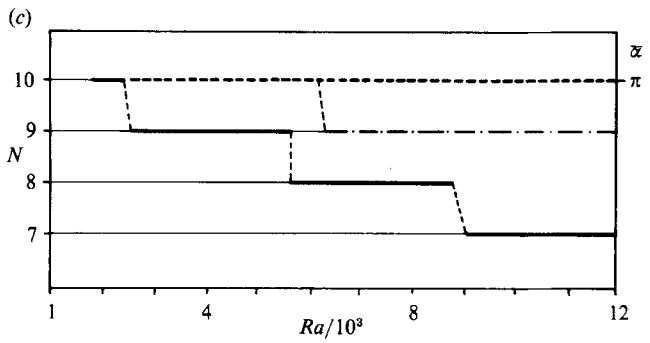

FIGURE 9. Wavelength of cellular convection in rectangular boxes. (*a*) Interferograms of steady cellular convection in water ($Pr = 7.0$). Aspect ratio = 10:4:1, $Ra = 3200, 6100, 8600, 42000$. (*b*, *c*) Average wave number a and number of cells N; ---, silicone oil ($Pr = 1780$); -·-·-, water ($Pr = 7.0$); ——, air ($Pr = 0.71$). Aspect ratio = 4:2:1 (*b*), = 10:4:1 (*c*).

vector can be considered as a measure of the flow's three-dimensionality (see figure 10*b*). The velocity profiles so represented result from the superposition of inertial and buoyancy forces. In the middle of the convection roll, we were able to observe an inwards-moving flow, while in the upward and downward motion areas, as a result of an axial pressure gradient, the fluid is transported towards the walls. The bulgings of the profiles are caused by the buoyancy-induced flows in the domain of strong horizontal temperature gradients. Since time-dependent solutions are largely determined by the Prandtl number, it must be assumed that secondary flows induced by the inertial forces, and not time-dependent disturbances, significantly determine the stability of steady cellular convection. Two points should be emphasized concerning the steady solutions in rectangular boxes: the flow field is influenced by nonlinear effects even in the regime of small supercritical Rayleigh number, see e.g. the transition in the wavelength and wavenumber. Further, in essential parts, the flow is highly three-dimensional and is characterized by a complex structure. Both features will significantly determine the transition to time-dependent solutions as will be shown in the following section.

6. Transition to oscillatory convection

In this section, we restrict ourselves to the 4:2:1 box (in order to keep computation time within limits) and to the case of a horizontal orientation of the box.

In experiments with air, no oscillations could be observed in the four-roll regime, since transition to a three-roll regime already took place at a Rayleigh number of 24000. This solution becomes unstable to time-dependent disturbances at a critical Rayleigh number of $Ra = 34000$, which agrees with the calculated onset of oscillations within the experimental error.

In the numerical calculations the number of cells is prescribed as input parameter due to the difficulties discussed in §5. According to the experimental observations the calculations are continued with a three-roll configuration for Rayleigh numbers higher than 24000.

Figure 11 presents the non-dimensional maximum vertical velocities as a function of the Rayleigh number. A comparison by Jäger (1982) of the calculated non-dimensional heat flux and the maximum vertical velocities, with measurements and

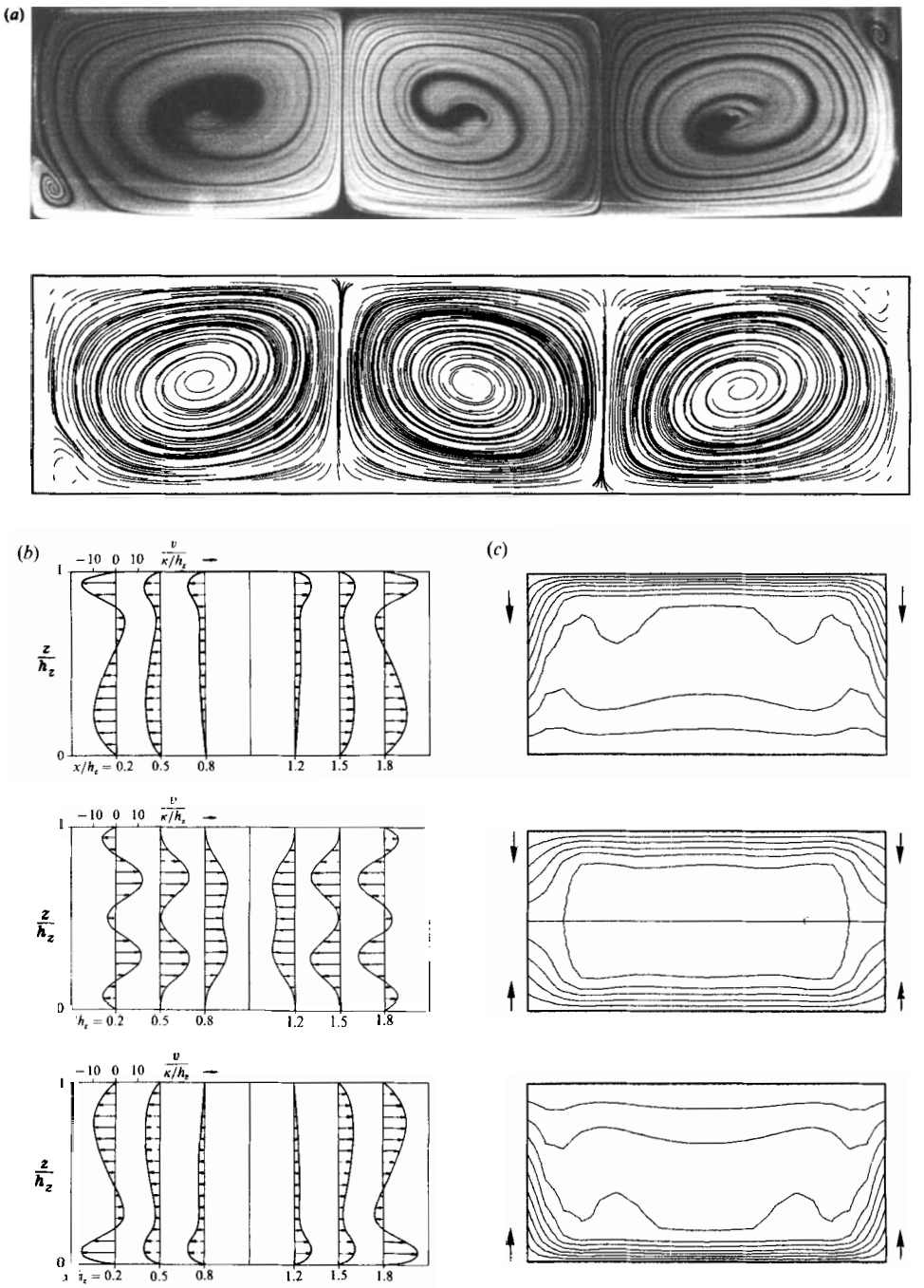

FIGURE 10. Steady cellular convection. $Ra = 30000$, $Pr = 0.71$, aspect ratio = 4:2:1. (*a*) Streakline photograph (Jäger 1982) and numerically integrated particle pathes (plane $y/h_z = 1.0$). (*b*) v-component of the velocity field at $x = 1.4$ (area of upward motion), $x = 2.0$ (middle of the cell) and $x = 2.6$ (area of downward motion). (*c*) Isotherms to figure 9(*b*).

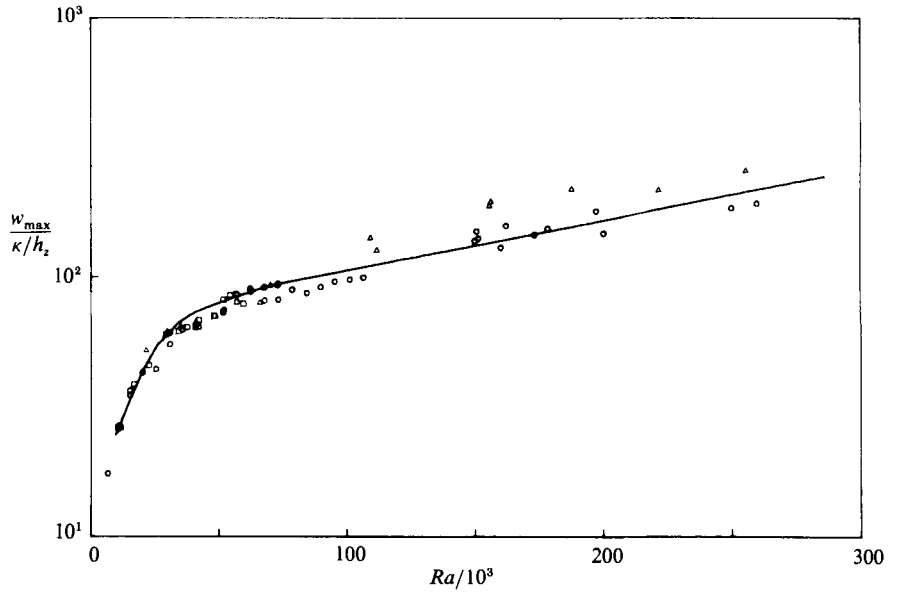

FIGURE 11. Vertical velocity component $w_{max}(x, y, z = 0.5)$. Aspect ratio = 4:2:1. ——, theory. Experiment: ○, air, $h_z = 39.5$ mm; □, air, $h_z = 24.0$ mm; △, water, $h_z = 8.4$ mm. (Jäger 1982).

otherwise published data, showed good agreement over the whole Rayleigh number range up to $Ra = 70000$, using a finite-difference method. In the range of Rayleigh numbers from 120000 to 200000, the application possibilities of the one-equation model of Prandtl and Kolmogorov, and in the range $Ra > 200000$, those of the (k, ϵ)-model, had been proven earlier using a finite-difference method. Nevertheless, the turbulence model applied could not reflect the flow structure and the correct oscillation frequencies.

We now concentrate on the transcritical transition regime to oscillatory instabilities and discuss the experimentally and theoretically determined Fourier spectra. Figure 12 shows the results of Fourier analysis in the form of experimental frequency spectra for different Rayleigh numbers, using the example of air as the test medium. First, the oscillations begin with a fixed frequency f_1. A second and a third frequency are added at a Rayleigh number of 50000. These are superimposed modulations of the original oscillations determined by the geometry of the box. With increasing Rayleigh number, the quasi-periodic regime of the route to turbulent convection is determined by the mode-locking $kf_1 + lf_2 + mf_3$ with integers k, l, m of the higher harmonics and their combination harmonics. The experiment shows that, at the Rayleigh number 52300, the oscillatory instability is again determined by the initial frequency f_1. With increasing Rayleigh number, there appear the sub-harmonics of f_2 and f_1, the period-doubling mechanism and the higher harmonic frequencies. The discrete mode-locking frequencies, determined by the Reynolds equations, can also be experimentally demonstrated in the turbulent regime. Similar results have been obtained by Gollub, Benson & Steinmann (1980). A quantitative comparison is however not possible because of the different geometry they have chosen in their experiments. The Galerkin method proved its advantage for the calculation of three-dimensional oscillatory convection. We assume symmetry of the flow with respect to the middle plane ($y = 0$), a fact which results in a limitation of the possible bifurcation solutions. The calculated oscillatory frequency f_1 (figure 13)

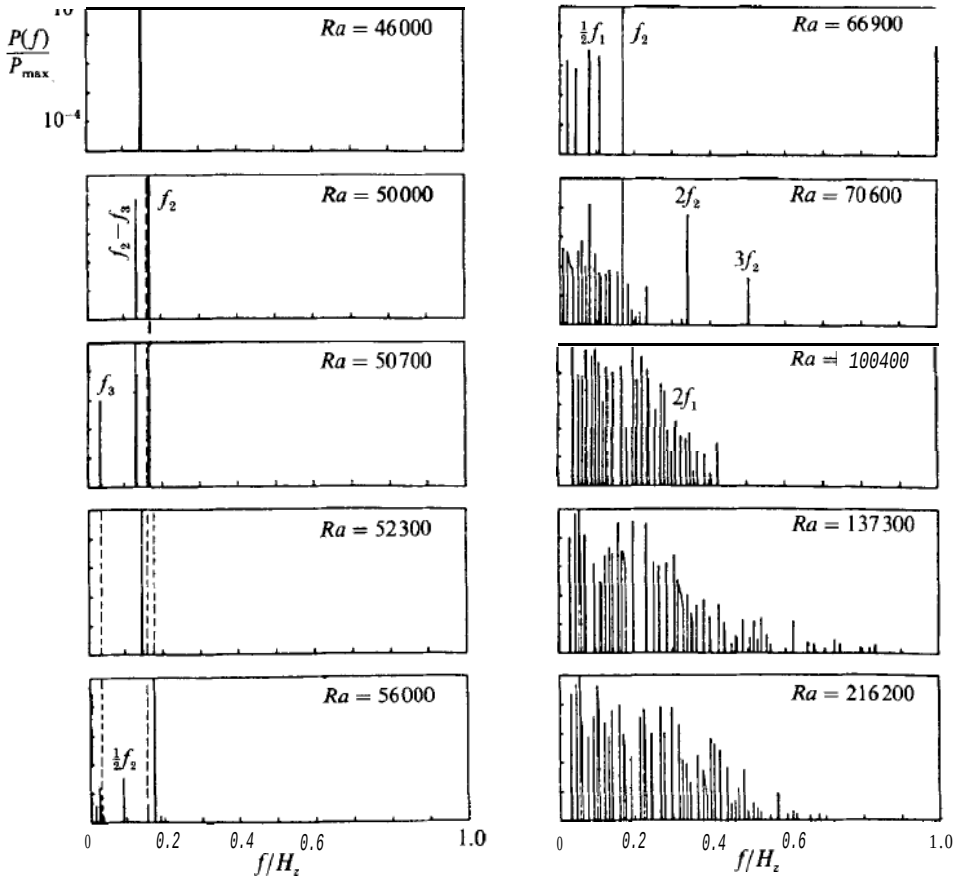

FIGURE 12. Experimental power spectra of the oscillatory convection in air Aspect ratio = 4 : 2 1. (Jäger 1982).

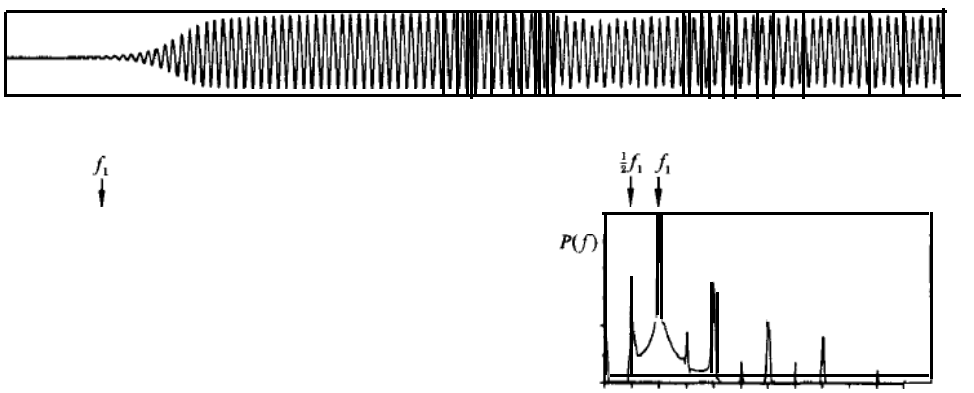

and the structure of the oscillatory convection are found to be in good agreement with experiments as discussed by Kessler *et al.* (1983). The numerical simulation demonstrates that changes of Prandtl number have a much stronger influence on the critical Rayleigh number of oscillatory convection, its frequency, structure and evolution in time and space than changes of the thermal boundary conditions at the sidewalls. The oscillations for air are completely different from those for water. For $Pr = 0.71$, the calculations exhibit large periodic contractions of the rolls, while for $Pr = 7$, the maximum amplitude of oscillation moves along the otherwise almost permanent rolls.

Going back to the frequency spectra of figure 13, in the comparison with experimentally determined frequency spectra, it can be noted that, for the basic frequencies f_1 and f_2, the subharmonics and higher harmonics are correctly reproduced, but the mode-locking details of the different frequencies cannot be resolved with the given numerical resolution and symmetry conditions.

7. Influence of shear flows

Under the influence of shear flow, caused e.g. by an inclination of the test box, the problem of thermal convection becomes more complex. The subcritical basic state is characterized by a single-roll convection flow, which influences the stability problem for onset of steady cellular convection with increasing angle of inclination. The supercritical convection itself results in a superposition of this basic flow and a cellular structure which makes the flow field highly three-dimensional.

7.1. *Onset of stationary cellular convection*

In order to test the stability calculations, discussed in §4, the onset of stationary cellular convection was experimentally investigated using interferometrical measuring methods. The characteristic stability behaviour (figure 14*a*, *b*) can be discussed in connection with example measurements made in silicone oil ($Pr = 1780$, $\delta = 15°$). On the left part of figure 14(*a*) is shown the (x, z)-plane, half the measuring cell consisting of an elementary diagram and half of an interferogram. In the right-hand column, we can see the short side of the box. The beam separation is horizontal, with reference to the measuring cell; thus a similarity between the interference fringes and streamlines can be derived in a slightly supercritical range.

The first interferogram describes the basic state. The fluid moves downwards at the colder upper wall and upwards at the warm lower wall. The fringe distribution shows that the simple assumption of the linear heat conduction profile in the basic flow fails at the vertical walls. In the box the solution is marked by an inhomogeneous v and T distribution, that is, the temperature and velocity fields not only depend on z but also on x and y.

The second interferogram shows the development of the first convection roll at the endwall, which already occurs in the range of subcritical Rayleigh numbers. The reason lies in the modified boundary condition, as compared with the classical stability theory. The basic flow causes both an upward and a downward motion at the vertical walls, forming a single convection roll. The fluid particles carry energy from the basic flow, facilitating an earlier onset of cellular convection near the endwalls. In a similar way subcritical motion can be induced by horizontal temperature gradients near the lateral wall (see e.g. Daniels 1977). One convection roll after the other now develops stepwise, beginning at the sidewalls and moving

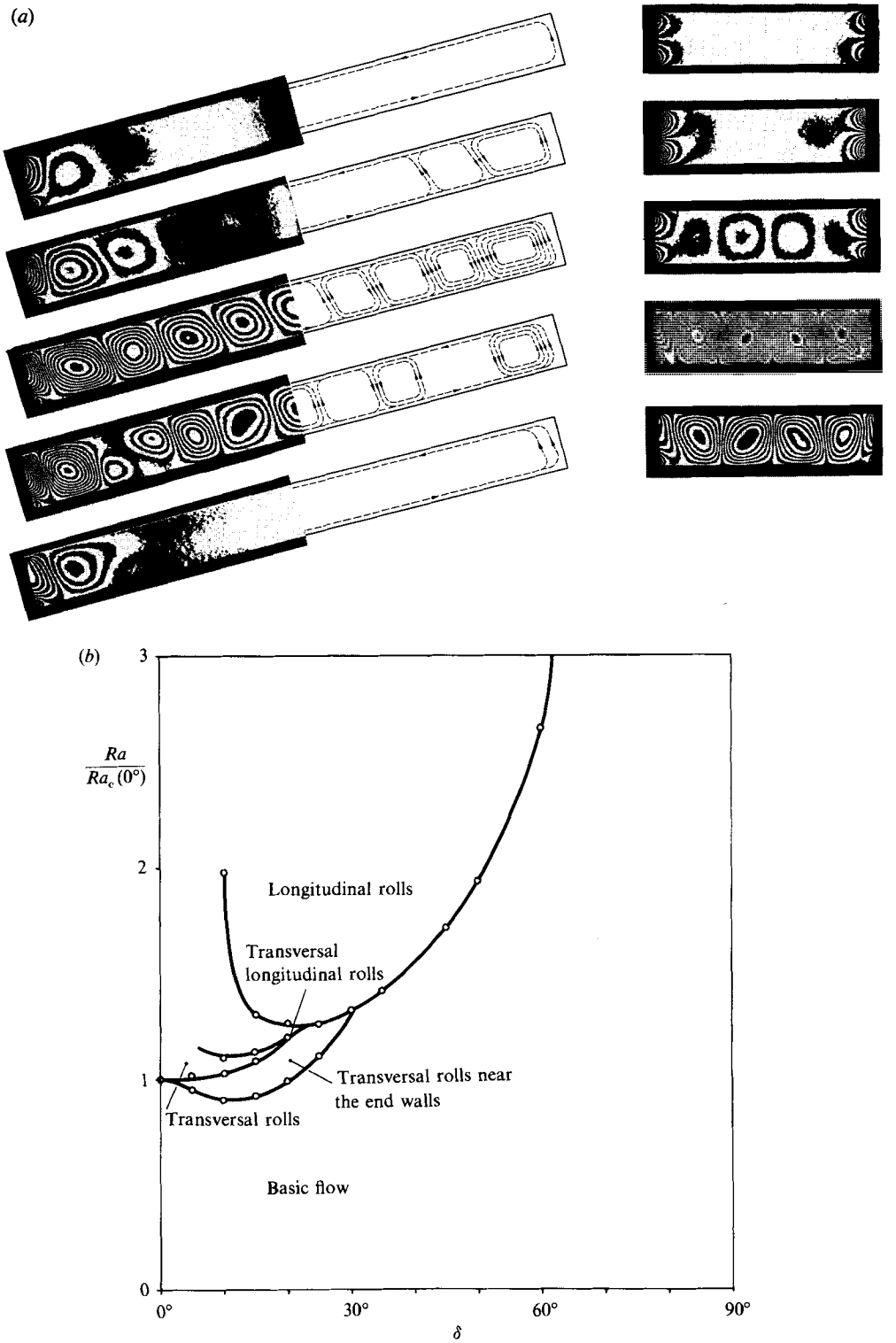

FIGURE 14. Steady cellular convection in silicone oil, $Pr = 1780$. (*a*) differential interferograms, $\delta = 15°$, $Ra = 1250, 1690, 2000, 2240, 2850$. (*b*) Critical Rayleigh numbers in a tilted box, aspect ratio $h_x : h_y : h_z = 10 : 4 : 1$. $Ra_c(0°) = 1820$.

towards the middle of the box. Consequently we do not observe a simultaneous onset of instability, as in the case of horizontal boxes, but because of the three-dimensional basic state we see an inhomogeneous development of cellular convection. In the third interferogram, a state is reached where the box is filled with convection rolls. This occurs approximately at the critical Rayleigh number predicted by the linear stability theory. Since the basic flow requires an upward motion at one of the endwalls and a downward motion at the other, only an odd number of cells – 9 in this particular case – is possible. As the interferogram on the right-hand side shows, a weak development of longitudinal rolls can already be recognized. The basic flow supports those rolls rotating in its own direction, but has a shear effect on those that rotate in the opposite one. This is unfavourable from the energetic point of view, and consequently, we can see how, with increasing Rayleigh number, the number of transverse rolls will slowly begin to decrease, doing so first of all in the middle of the box. At the same time, longitudinal rolls begin to develop along the basic flow, which becomes stronger. At a Rayleigh number of 2850, we finally find a state in which only longitudinal rolls are superimposed on the basic circulation. The flow made up of u, w and v, w motions is now highly three-dimensional, with single fluid particles moving in complex spiral paths.

The results of all single tests with silicone oil are summarized in the stability diagram in figure 14. The Rayleigh number is normalized at the critical value necessary for the onset of transverse rolls when $\delta = 0°$, $Ra_c(0°) = 1816$. The angles of inclination $\delta = 0°$ to 90° are plotted on the x-coordinate. Three domains can be recognized in the stability diagram. A complex stability behaviour can be observed from 0° to 30°. Transverse rolls appear close to the wall even at subcritical Rayleigh numbers, being identical with the rolls parallel to the shorter side of the box. These rolls appear as a result of basic flow's modified boundary conditions. The next curve is, in our view, the real stability curve; cellular convection starts to be present in the entire box here. The values thus determined are comparable with the theoretical predictions as shown in figure 6 (for small angles there is only a weak influence of the Prandtl number). With increasing Rayleigh number, the basic flow gains influence and forces the roll structure to reorient itself. Within a limited parameter range, there is a practical superposition of two types of rolls. This state is stable, that is, the rolls will remain unchanged for any time interval, as long as the Rayleigh number is not modified. Only when the basic flow has reached a certain amplitude do pure longitudinal rolls develop in the same way as from infinitely extended layers. This flow picture also characterizes the second range, from 30° to 65°. Finally, the critical Rayleigh number increases steeply with increasing angle of inclination. The cellular convection will lose significance to the same extent as the basic flow increases in amplitude. Above $\delta = 65°$, it is no longer possible to detect any convection rolls on the interferogram. The convective transport of energy is taken over solely by the very strong basic flow.

Further results concerning the onset of cellular motion are included in figures 17 and 19 for the Prandtl numbers 0.71 (air) and 7.0 (water). After comparing with the theoretical predictions we can summarize the results as follows: the subdivision into transverse and longitudinal rolls, depending on the angle of inclination, is reflected satisfactorily. For small angles, the value of the critical Rayleigh number agrees, within the experimental error, with theoretical predictions. However, for angles of $\delta > 50°$, there deviations appear which reach 60% in the extreme case. In general terms, we can say that the critical Rayleigh number determined experimentally is higher. One reason for this may be found in a systematic error measurement caused

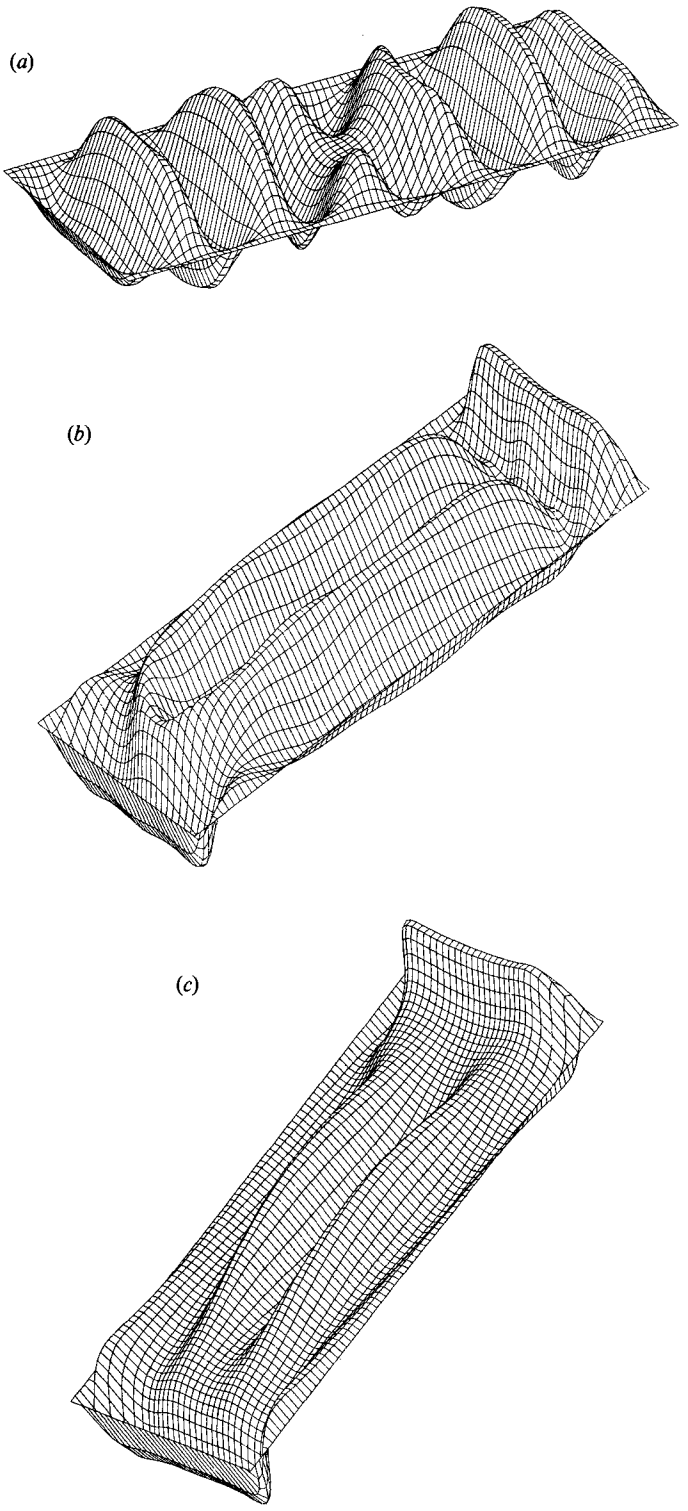

FIGURE 15(a–c). For caption see facing page.

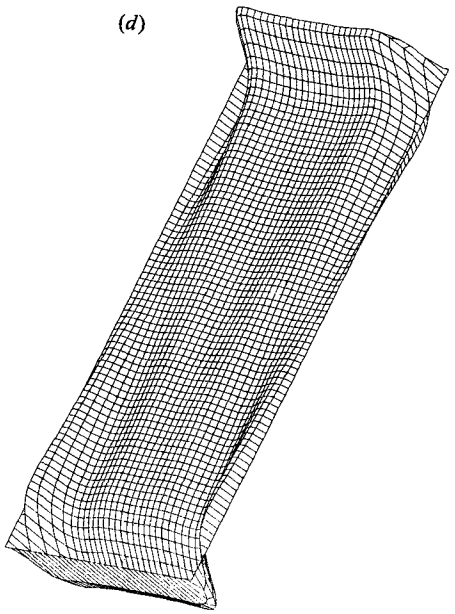

FIGURE 15. Three-dimensional convection in tilted boxes. Aspect ratio = 10:4:1, $Pr = 7.0$. Distribution of the vertical velocity component in the plane $z = 0.5$. (*a*) $\delta = 5°$, $Ra = 3010$; (*b*) $\delta = 30°$, $Ra = 3464$; (*c*) $\delta = 50°$, $Ra = 4670$; (*d*) $\delta = 60°$, $Ra = 6000$.

by the application of measuring methods of different sensitivity. The error is due to the fact that only a finite flow amplitude can be observed, which prevents registration of the first infinitesimal deviation of the basic state. The experimentally determined Rayleigh number will, therefore, always be somewhat higher, increasing with decreasing sensitivity of the interferometer used. An additional effect appears above $\delta = 50°$. The entire flow is formed by the superposition of basic circulation and cellular convection. The stability calculation gives no information about the ratio of amplitude of the two flow parts. The interferograms taken during the experiment show that the flow part with cellular convection decreases continually with increasing angle of inclination and stronger basic flow. Three-dimensional calculation of the supercritical flow conditions has also confirmed this observation. This demonstrates why, above $\delta = 65°$, cellular structures can no longer be observed in what has now become a very strong basic flow. Therefore, in the case of moderate aspect ratio containers, the eigenvalues obtained with the linear stability theory have only theoretical significance for large angles of inclination, giving no meaningful information about the physical facts.

7.2. *Supercritical steady solutions*

In order to reach a better understanding of the spatial structure of convection in tilted boxes, a calculation of the supercritical flow field was carried out for a number of selected examples. The results are presented in figure 15 as the distribution of the vertical velocity component in the plane $z/h_z = 0.5$. The Prandtl number was fixed at the value of 7.0. In addition, the component of the Rayleigh number in the z-direction was kept constant at $Ra_z = 3000$, which means that the actual Rayleigh number changes with the angle of inclination δ, following the relation $Ra = 3000/\cos\delta$.

When the angles of inclination are small and a weak basic flow is present, the

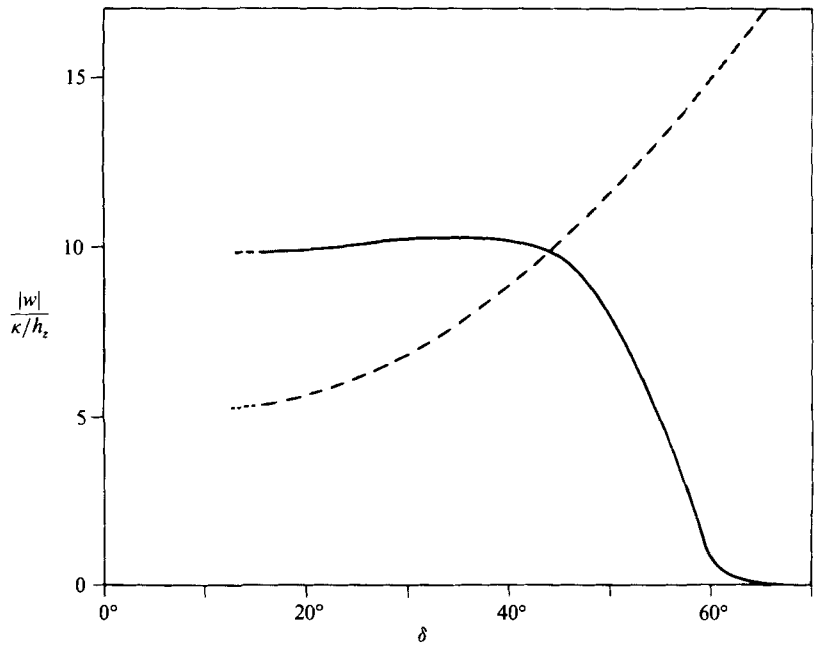

FIGURE 16. Amplitude of cellular convection and basic flow in inclined boxes. $Pr = 7.0$, aspect ratio = 10:4:1. ——, $w(x = 5, y = 2, z = 0.5)$; – – –, $w(x = 9.75, y = 2, z = 0.5)$.

transverse rolls have the smaller eigenvalue and are thus the preferred solution (figure 15*a*). However, a marked deviation from the roll structure can already be seen at the centre of the box. This suggests the reorientation to longitudinal rolls which takes place at larger angles of inclination. This solution, which results from the superposition of the basic flow and four rolls lying perpendicularly to it, is represented in figure 15 (*b*) for $\delta = 30°$. If the angle of inclination is further increased, the intensity of the basic flow will increase steadily, while the amplitude of the cellular convection will decline noticeably. At $\delta = 50°$, partial cellular convection can still be detected in the middle of the box. From $\delta = 60°$–$65°$, there remains only a strong basic circulation, which controls the entire energy transport (figure 15*d*).

By way of example, the two representative velocity profiles in figure 16 show once again how basic flow and cellular convection vary with increasing angle of inclination. $w(x = 9.75, y = 2, z = 0.5)$ is close to the upper endwall and serves as a measure of the basic flow's intensity. $w(x = 5, y = 2, z = 0.5)$ lies in the area of downstream motion right in the middle of the box and characterizes the part with cellular convection. Upwards of $\delta \approx 45°$, the amplitude of the cellular convection decreases strongly, and from $\delta = 65°$, there is only a basic flow left. In fact, a modulation $w(y)$ is still detectable in the middle of the box at $\delta = 65°$, but the amplitude reaches only 0.25 % of the original convection rolls. The results make the differences between the experimental and theoretical investigations clear. Consistent with the above, an eigenvalue is calculated for the angle of inclination $\delta = 65°$ (see figure 6), as the numerical results still show a periodic distribution $w(y)$, but with a negligibly small amplitude. The fact that the cellular convection cannot be measured in this range, even with sensitive optical measuring methods, is also understandable.

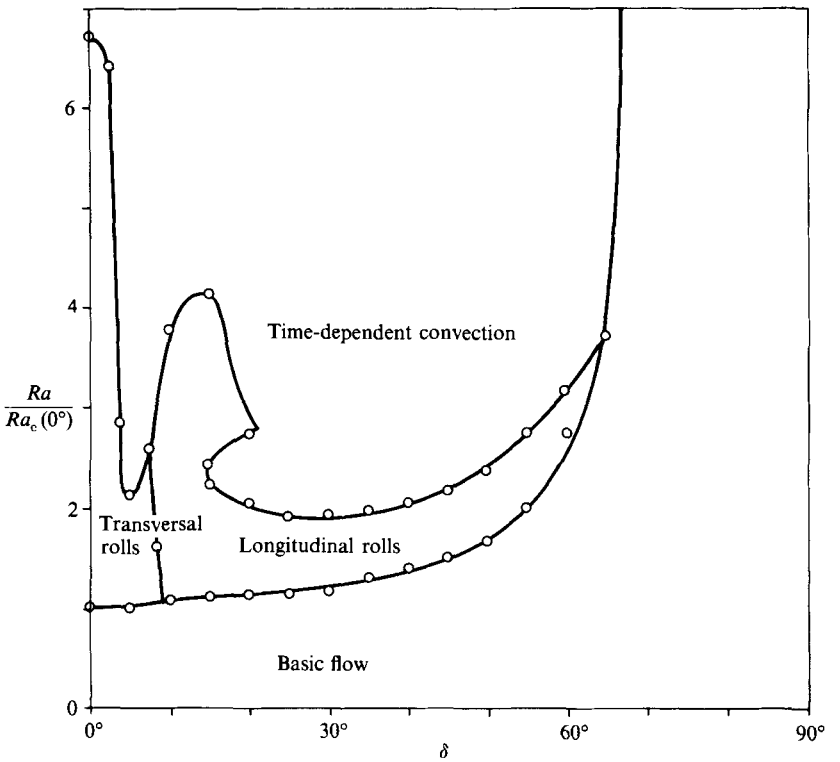

FIGURE 17. Stability diagram in air, $Pr = 0.71$, aspect ratio = 10:4:1. Experimental results.

7.3. *Onset of time-dependent convection*

Another important problem is the onset of time-dependent solutions, which we shall discuss using the experiments' stability diagrams for water ($Pr = 7.0$) and air ($Pr = 0.71$). Figure 17 shows the stability diagram for nitrogen. The lowest curve indicates the onset of stationary cellular convection in a simplified form (the appearance of subcritical motions for small angles of inclination is omitted). We will now concentrate on the transition curves of the time-dependent solutions. In a horizontal box, oscillatory convection sets in at a Rayleigh number that is about seven times supercritical. A wave is hereby superimposed on the rolls in the axial direction, causing periodic variations in the flow field. If we incline the box slightly, the transverse rolls will become unstable at a much lower Rayleigh number. The shear forces caused by the basic flow induce time-statistical reorientations of the upward and downward motion areas. At angles of inclination of $\delta > 10°$, the rolls will orient along the basic flow, avoiding a shear effect. This has an immediate stabilizing influence on the onset of time-dependent solutions. From $\delta = 15°$ on, oscillatory convection sets in at a lower Rayleigh number level, which means that, here too, the basic flow has a clear destabilizing effect on the convection rolls in relation to time-dependent solutions. If we define a modified Rayleigh number as $Ra^* = Ra \cos\delta$, oscillations for the angle range of 15° to 60° set in at an almost constant value of $Ra^* = 2900 \pm 100$. Obviously, only the z-component of the gravitational acceleration, $g_z = g \cos\delta$, is important for the transition to time-dependent solutions in this angle range.

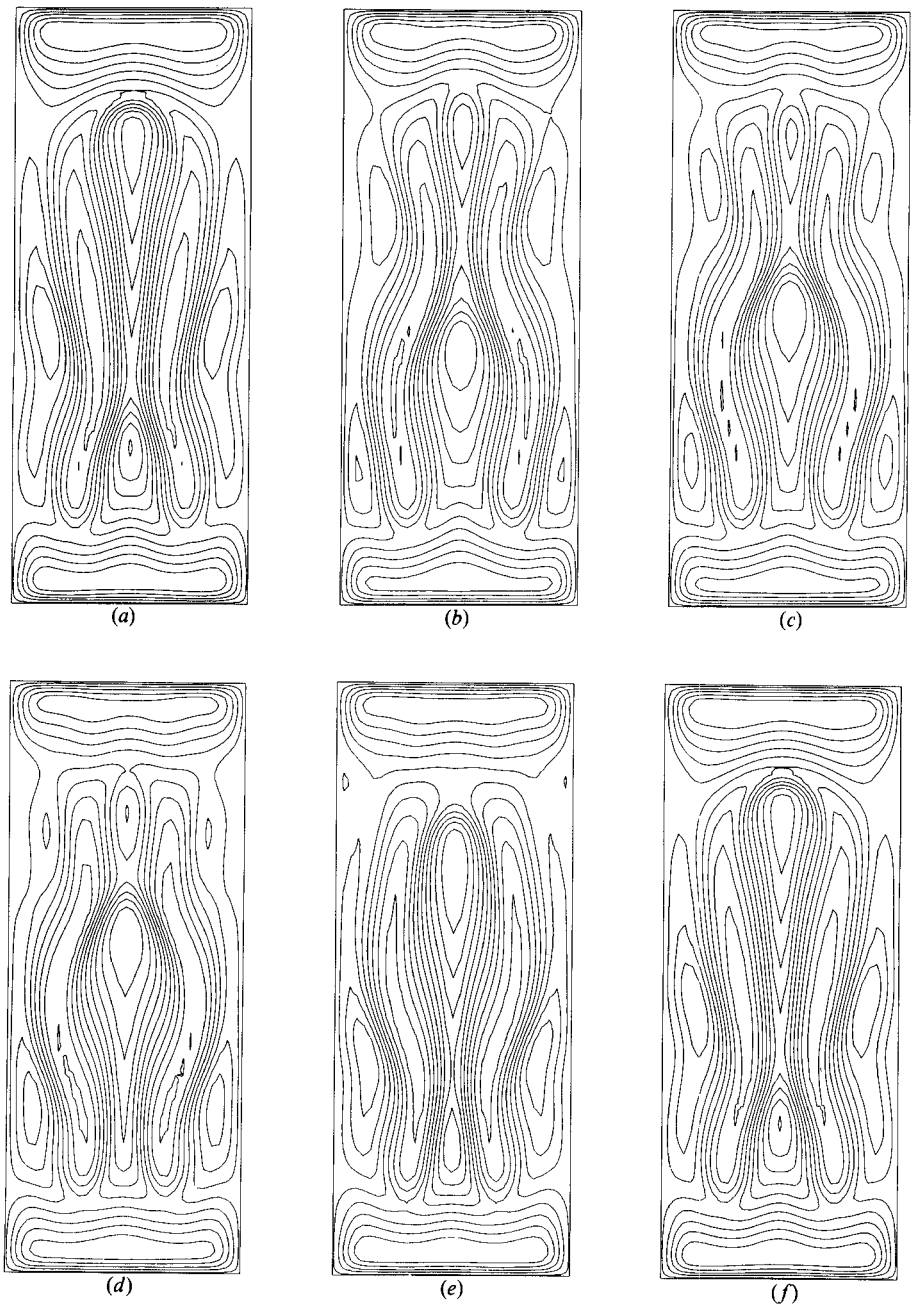

FIGURE 18. Oscillatory convection $\delta = 40°$, $Ra = 4500$, $Pr = 0.71$, aspect ratio = 10:4:1. Isotherms in the plane $z = 0.5$. (*a*) $t = 7.010$; (*b*) $t = 7.155$; (*c*) $t = 7.196$; (*d*) $t = 7.237$; (*e*) $t = 7.311$; (*f*) $t = 7.381$.

The physical model and the numerical method are tested by means of a selected example, to determine if they also correctly describe the oscillatory convection in tilted boxes. At an angle of inclination of $\delta = 40°$, and from the Rayleigh number $Ra = 3900$ onwards, it is no longer possible to calculate a stationary solution. This value lies slightly above the experimentally determined critical Rayleigh number of

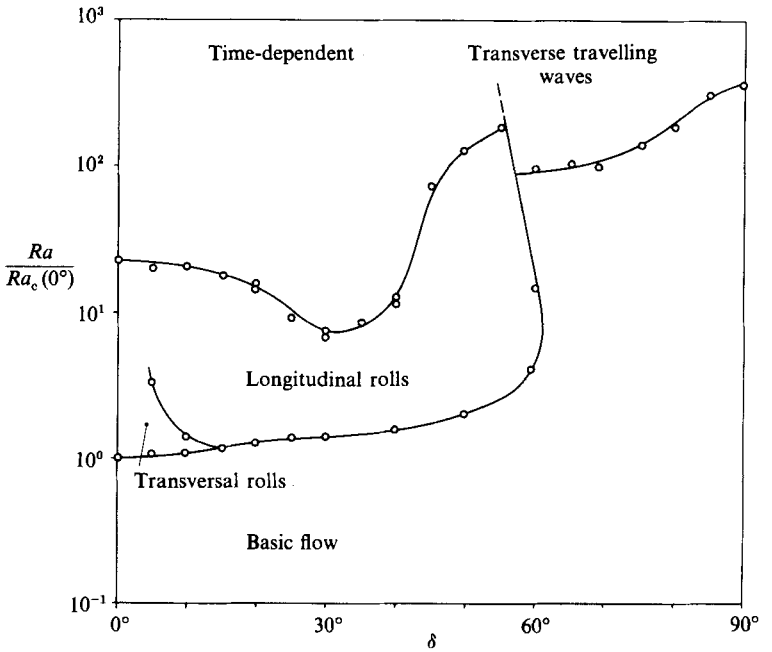

FIGURE 19. Stability diagram in water, $Pr = 7.0$, aspect ratio = 10:4:1. Experimental results.

$Ra_{osc} = 3700$. In order to shorten the transition phase and save computing time, the oscillations are calculated for a slightly supercritical Rayleigh number of $Ra = 4500$.

The temporal change of the flow structure is illustrated by the distribution of isotherms in the plane $z = 0.5$ (figure 18). The momentary isotherm field was drawn over a period of oscillation taking six different points in time. A wave can be clearly recognized, which moves along the axes of the rolls, causing a periodic displacement of the upward and downward motion areas, as well as a modulation of the flow's amplitude. When the cross-section of the rolls becomes smaller, the flow's amplitude enlarges, and conversely, when it spreads, the flow's amplitude becomes smaller. This agrees with experimental observations carried out with the aid of streak-line pictures. The dimensionless frequency is 2.67, deviating 8% from the experimentally determined value ($f_{exp} = 2.45$). Altogether, we can say that the three-dimensional finite-difference method, in the main, correctly describes the experimentally observed behaviour of oscillatory convection. Water was another of the test fluids investigated; the corresponding results are summarized in figure 19. Similarly to the results already discussed for silicone oil and nitrogen, a distribution among transverse and longitudinal rolls was also found in water. The onset of oscillatory convection for $\delta = 0°$ is first measured at a Rayleigh number of $Ra = 42000$.

Here, too, we have established that, for angles of inclination of up to $\delta = 35°$, the basic flow has an increasingly destabilizing effect on the onset of time-dependent solutions. However, the effect is not as marked as in nitrogen. Above this angle of inclination, the critical Rayleigh number required for the onset of time-dependent convection increases steeply again. This effect is influenced by the mutual action of the z and x components of the gravitational term. The influence of cellular convection will prevail at small angles of inclination. The perturbations which induce the transition to time-dependent convection are induced by the basic flow. At larger angles, it is the basic flow that prevails, being even extremely stable against time-

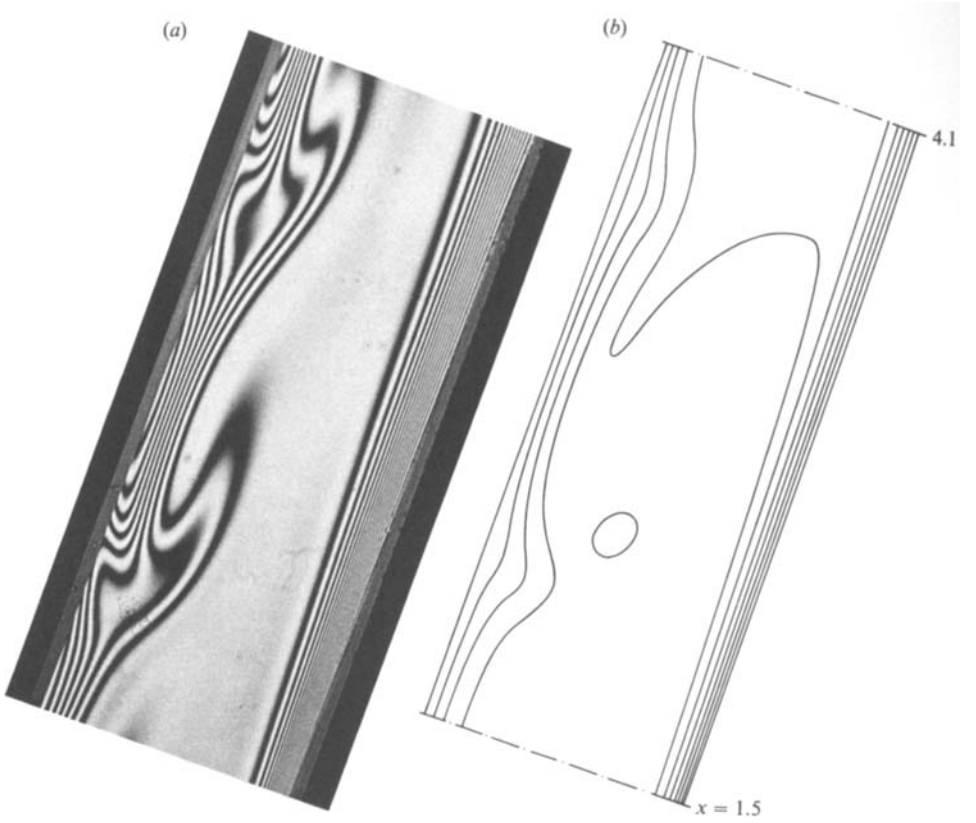

FIGURE 20. Transverse travelling waves. $Ra = 4.3 \times 10^5$, $Pr = 7.0$, $\delta = 70°$, aspect ratio = 10:4:1. (*a*) Differential interferogram. (*b*) Evaluated isotherms lines with $T = 1.0, 0.9, 0.8, 0.7, 0.6, 0.5, 0.4, 0.3, 0.2, 0.1, 0$.

dependent perturbations. From $\delta = 60°$ on, cellular convection can no longer be measured. A steady basic circulation is only present up to a Rayleigh number of 1.8×10^5. This basic circulation becomes unstable above the plotted curve in the form of transverse travelling waves.

These transverse travelling waves can be considered as a shear instability. After a build-up distance of $x/h_z = 4$–8, and depending on the angle of inclination, waves develop in the boundry layers with a phase velocity of about the order of magnitude of the maximum flow velocity. When the flow deflects at the endwalls, the waves die out, developing again at the opposite side after a new build-up distance. The appearance of the transverse rolls was measured with the highly sensitive laser differential interferometer, as the amplitude of the waves is extremely small very close to the box's vertical walls and cannot be measured with a total-field differential interferometer.

Above $\delta = 60°$, we were able to observe a periodic oscillation of the temperature field at the critical point indicating the onset of transverse waves. The value of the critical Rayleigh number at $\delta = 90°$ is 6.7×10^5 and may be directly compared with the predictions made by Elder in 1965. For the case of an almost plane flow, Elder made an estimation of the form $Ra = 8 \times 10^8 Pr^{\frac{1}{2}}/H_x$, which leads to a value of 1.97×10^6 for the present container and the test medium water ($Pr = 7.0$). Our own measurements lie considerably below this value, in spite of the stabilizing effect of the

sidewalls. We suspect that the first onset of transverse rolls could not be observed with the visualization methods used until now and that, therefore, the values of the critical Rayleigh numbers were too high.

Figure 20(*a*) shows an interferogram as cut out from the measuring cell. At the cold wall, the curvature of the interference fringes allows detection of the existence of waves in the temperature boundary layer, whereas at the warm wall, after the deflection at the sidewalls, the boundary layer remains laminar at first. A quantitative evaluation of the interferograms gave the isothermal distribution presented in figure 20(*b*).

8. Discussion and conclusions

The present paper reports a combined experimental and theoretical investigation of three-dimensional convection in horizontal and tilted boxes of moderate aspect ratio.

For the case $\delta = 0°$, the linear stability theory describes the onset of steady cellular convection, in agreement with experimental observations. Special attention must be paid to a careful selection of the trial function for the series expansion of the unknown functions v and T. In tilted boxes, however, the stability problem becomes much more complicated, because of the highly inhomogeneous basic state, which itself is a three-dimensional flow. The novel aspect of this work is the combination of a Galerkin method and a finite difference scheme in solving the stability problem, a procedure which is undoubtedly necessary for the aspect ratios used in our investigations. There are some fundamental differences between the stability behaviour of cellular convection in tilted and horizontal boxes. First, subcritical motion arises in the neighbourhood of the lateral walls comparable to the case with a small heat flux through the sidewalls (see Daniels 1977), but with a significantly higher intensity.

Depending on the aspect ratio, transverse rolls are the preferred solution for small angles, a fact which is not mentioned in earlier published works, e.g. of Hart (1971). The stability analysis correctly describes the existence of transverse and longitudinal rolls and the transition angle between these two modes. Finally the Prandtl number is introduced in the stability problem by the coupling mechanism between the basic flow and cellular convection. Thus the critical Rayleigh numbers show a weak dependence on the Prandtl number. Our own results are compared with the publication of Hart (1971), one of the first systematic investigations of convection flow and stability phenomena in inclined boxes. Although he used large aspect ratio geometries ($h_x : h_y : h_z = 25 : 12 : 1$ and $37 : 17 : 1$) the essential parts of his results are qualitatively confirmed by our investigations. On the other hand, there are remarkable details which are different and which underline the influence of the lateral walls and of nonlinear effects:

(i) The rolls parallel to the shorter side of the box do not disappear immediately when the box is inclined some degree from the horizontal position.

(ii) The appearance of meanders on the longitudinal vortices before unsteadiness occurs is obviously suppressed by the influence of the lateral walls.

(iii) The transition angle between cellular convection and a single roll configuration is shifted to smaller values with decreasing aspect ratio. The measured transition angle of $\delta = 65°$ agrees with the result of Arnold, Catton & Edwards (1976), who published a relationship between this angle and the aspect ratio by means of heat transfer measurements.

(iv) The transverse travelling waves exist at significantly smaller Rayleigh numbers than observed in the experiments of Hart and in the relationship given by Elder (1965). This relationship neglects the three-dimensional effects in the basic flow, which obviously has a destabilizing effect on the transition to travelling waves.

Finally, we will emphasize that the steady and time-dependent solutions of cellular convection in boxes of intermediate aspect ratio is sensitively influenced by the lateral walls.

Let us return to the supercritical convection in horizontal boxes. One of the most interesting features of cellular convection is the increase of the wavelength, that is in a closed box, a decrease in the number of cells to higher Rayleigh numbers. A great number of published experimental observations, including the results presented in this paper, unequivocally show this effect. The transition Rayleigh numbers, which sensitively depend on the Prandtl number and the aspect ratio, are reproducible in a great number of experimental runs, assuming the same initial conditions. Although the numerical simulations of the steady solutions reflect the mean features of the flow correctly, e.g. the flow amplitude and flow structure and also integral properties such as the Nusselt number, it was not possible to calculate transitions in the number of cells. Similar results are reported by other authors. Upson *et al.* (1983) attempted in vain, by using different perturbations of the temperature field, to force a bifurcation from a three- to a two-cell configuration as was observed in the experiments of Maurer & Libchaber (1979).

This result is surprising, because other complicated three-dimensional reorientations of the flow structure are reproduced with considerable agreement to the experiments. One example, presented in this paper, is the transition from transversal to longitudinal convections rolls in tilted boxes (see figure 15). What is the reason for this contradiction? Our experiments in air indicate that the transition in the cell number is characterized by a long-time transient reorientation of the whole flow field, needing several units of the thermal diffusion time. The experiments of Kolodner *et al.* (1986) with water as the test fluid can be interpreted in a similar way. But even with the use of vector computers it is impossible to simulate such a transition, for which many hours of CPU-time could be needed.

For the simulation of the time-dependent solution, the number of cells observed in the experiment must be given as input parameters since the critical Rayleigh number, for the onset of oscillations as well as the dynamical behaviour, is a function of the subcritical steady solution (see e.g. Clever & Busse 1974). In this way the critical Rayleigh number and the oscillation frequency is correctly reproduced and in good agreement with the experiments of Jäger (1982). Further, the results obtained with the finite-difference method agree in the main features with the publication of Kessler, who used a Galerkin method and applied it to a box with an aspect ratio of $4:2:1$; however some difference must be mentioned, concerning the dynamical behaviour of the oscillatory convection. In the simulations of Kessler, the axis of the middle roll (in a three-roll configuration) remains fixed through an oscillation period. However the finite difference calculations yield an oscillation of this axis similar to the axis of the two outer rolls. Repeating the experiments of Jäger we could indeed observe, that the axis of the centre roll oscillates in a way prescribed by the finite-difference method. It seems, that the symmetry condition that Kessler imposed on his method led to some restrictions in the dynamical behaviour. It is surprising that this has no influence on the oscillation frequency.

Our calculations confirm the statement of Kessler, that for a box of intermediate

aspect ratio the thermal boundary conditions only slightly influence the onset of oscillatory instability as well as the frequency and the dynamical behaviour, although there are noticeable modifications in the spatial flow structure. More important are the nonlinear effects characterized by the Prandtl number. It should be mentioned, that this statement is not generally valid for the whole range of aspect ratios. Recent calculations of the authors (Kirchartz 1987) in cubical boxes, heated from below, demonstrate, that with decreasing aspect ratio, i.e. with increasing influence of the lateral wall, the above conclusion can be changed drastically. The dynamical behaviour of the time-dependent convection, including the critical Rayleigh numbers, are mainly influenced by the thermal boundary condition (perfectly conducting or adiabatic), while the influence of the Prandtl number is of second order.

As a result of our work, we should emphasize that the transition to a time-dependent solution is largely determined by the three-dimensional effects. Inertial and buoyancy forces cause marked spatial flow movement not only in the immediate neighbourhood of the lateral walls, but also influence the whole flow field. Thus the oscillatory convection could only be calculated with the aid of a three-dimensional model. The critical Rayleigh number, the oscillation frequency and the qualitative picture of the flow pattern agree with the experimental observations.

This work was conducted by the authors at the Institut für Strömungslehre und Strömungsmaschinen, University of Karlsruhe. We would particularly like to thank Professor Dr-Ing. J. Zierep, who encouraged and stimulated the investigations with many suggestions. This work also benefited from discussions with W. Jäger and R. Kessler. The work received financial support from the Deutsche Forschungsgemeinschaft. The numerical calculations were carried out in the computing centres at the DFVLR and the University of Karlsruhe.

REFERENCES

ARNOLD, J. N., CATTON, I. & EDWARDS, D. K. 1976 *J. Heat Transfer* **98**, 67–71.

BOSSEL, H. H., HILLER, W. J. & MEIER, G. E. A. 1972 *J. Phys.* E **5**, 893–896.

BUSSE, F. H. 1978 *Rep. Prog. Phys.* **41**, 1929–1967.

BUSSE, F. H. 1981 Transition to turbulence in Rayleigh–Bénard convection. In *Hydrodynamic Instabilities and the Transition to Turbulence* (ed. H. L. Swinney & J. P. Gollub), pp. 97–133. Springer.

CATTON, I. 1970 *J. Heat Transfer* **92**, 186–188.

CATTON, I. 1978 *Proc. of the 6th Intl Heat Transfer Conf. Toronto*, pp. 13–30.

CHANDRASEKHAR, R. S. 1961 *Hydrodynamic and Hydromagnetic Stability*. Oxford University Press.

CLEVER, R. M. & BUSSE, F. H. 1974 *J. Fluid Mech.* **65**, 625–645.

CLEVER, R. M. & BUSSE, F. H. 1977 *J. Fluid Mech.* **81**, 107–127.

CLEVER, R. M. & BUSSE, F. H. 1978 *Z. angew. Math. Phys.* **29**, 711–714.

CURRY, J. H., HEERING, J. R., LONCARIC, J. & ORZAG, S. T. 1984 *J. Fluid Mech.* **147**, 1–38.

DANIELS, P. G. 1977 *Proc. R. Soc. Lond.* A **358**, 173–197.

DAVIS, S. H. 1967 *J. Fluid Mech.* **30**, 455–478.

ELDER, J. W. 1965 *J. Fluid Mech.* **23**, 99–111.

GERSHUNI, G. Z. & ZHUKHOVITSKI, E. M. 1976 *Convective Instability in Incompressible Fluids*. Keter Publishing House.

GOLLUB, J. P., BENSON, S. V. & STEINMANN, J. 1980 *Ann. N.Y. Acad. Sci.* **357**, 22–27.

HARRIS, D. L. & REID, W. H. 1958 *Astrophys. J. Supp.* **3**, 429–453.

HART, J. E. 1971 *J. Fluid Mech.* **47**, 547–576.

HOLLANDS, K. G. T. & KONICEK, L. 1973 *Intl J. Heat Mass Transfer* **16**, 1467–1476.

JÄGER, W. 1982 Oszillatorische und turbulente Konvektion. Diss. University Karlsruhe, West Germany.

JOSEPH, D. D. 1976 *Stability of Fluid Motion*, vol. 1, vol. 2. Springer.

KESSLER, R. 1984 *DFVLR-FB* 84-14.

KESSLER, R. 1987 *J. Fluid Mech.* **174**, 357–379.

KESSLER, R., DALLMANN, U. & OERTEL JR, H. 1983 *Proc. of IUTAM-Symposium on Turbulence and Chaotic Phenomena in Fluids*, pp. 173–178.

KIRCHARTZ, K. R. 1980 Zeitabhängige Zellular konvektion in horizontalen und geneigten Behältern, Diss. University Karlsruhe, West Germany.

KIRCHARTZ, K. R. 1987 *Z. angew. Math. Mech.* **67**, T293–T296.

KIRCHARTZ, K. R., OERTEL JR, H. & ZIEREP, J. 1982 Time-dependent convection. In *Convective Transport and Instability Phenomena*, pp. 101–122. Braun.

KOLODNER, P., WALDEN, R. W., PASSNER, A. & SURKO, C. M. 1986 *J. Fluid Mech.* **163**, 195–226.

KOSCHMIEDER, E. L. 1974 *Chem. Phys.* **26**, 177–211.

LINTHORST, S. J. M., SCHINKEL, W. M. & HOOGENDOORN, C. J. 1981 *J. Heat Transfer* **103**, 535–537.

LIPPS, F. B. 1976 *J. Fluid Mech.* **75**, 113–148.

MAURER, J. & LIBCHABER, A. 1979 *J. Phys. Lett. Paris* **40**, 419–423.

NAGATA, M. & BUSSE, F. H. 1983 *J. Fluid Mech.* **135**, 1–26.

NORMAND, C., POMEAU, Y. & VELARDE, M. G. 1977 *Rev. Mod. Phys.* **49**, 581–624.

OERTEL, H. 1961 *ISL Technische Mitteilung* T17/61.

OERTEL JR, H. 1979 Thermische Zellularkonvektion. Habilitation University Karlsruhe, West Germany.

OERTEL JR, H. 1980 *Natural Convection in Enclosures* (ed. I. Catton & K. E. Torrance). ASME HTD, vol. 8, 11–16.

OERTEL JR, H. 1984 In *Nonlinear Dynamics of Transcritical Flow* (ed. H. L. Jordan, H. Oertel jr and K. Robert), pp. 1–36.

OERTEL JR, H. & BÜHLER, K. 1978 *Intl J. Heat Mass Transfer* **21**, 1111–1115.

OERTEL, H. & OERTEL JR, H. 1988 *Optische Strömungsmeßtechnik*. Braun.

OZOE, H., FUJII, K., LIOR, N. & CHURCHILL, S. W. 1983 *Intl J. Heat Mass Transfer* **26**, 1427–1438.

OZOE, H., SAYAMA, H. & CHURCHILL, S. W. 1977 *Intl J. Heat Mass Transfer* **20**, 123–129.

PALM, E. 1975 *Ann. Rev. Fluid Mech.* **7**, 39–61.

PIACSEK, S. A. & WILLIAMS, G. P. 1970 *J. Comp. Phys.* **6**, 392–405.

PLATTEN, J. K. & LEGROS, J. C. 1984 *Convection in Liquids*. Springer.

RICHTMYER, R. D. & MORTON, K. W. 1967 *Difference Method for Initial-Value Problems*. Interscience.

ROACHE, P. J. 1972 *Computational Fluid Dynamics*. Hermosa.

ROBERTS, P. M. 1975 *Adv. Chem. Phys.* **32**, 17–32.

RUTH, D. W., HOLLANDS, K. G. T. & RAITHBY, G. D. 1980*a* *J. Fluid Mech.* **96**, 461–492.

RUTH, D. W., RAITHBY, G. D. & HOLLANDS, K. G. T. 1980*b* *J. Fluid Mech.* **96**, 481–492.

SCHUMANN, U. 1976 *Comp. Phys.* **20**, 171–182.

STORK, K. & MÜLLER, U. 1972 *J. Fluid Mech.* **54**, 599–611.

SWINNEY, H. L. & GOLLUB, J. P. 1981 Hydrodynamic Instabilities and the Transition to Turbulence. Springer.

TURNER, J. S. 1973 *Buoyancy Effects in Fluids*. Cambridge University Press.

UNNY, T. E. 1972 *J. Appl. Mech.* **94**, 41–46.

UPSON, C. D., GRESHO, P. M., SANI, R. L., CHAN, S. T. & LEE, R. L. 1983 In *Numerical Properties and Methodologies in Heat Transfer*, pp. 245–259. Hemisphere.

ZIEREP, J. 1963 *Beitr. Phys. Atmos.* **36**, 70–76.

ZIEREP, J. & OERTEL JR, H. 1982 *Convective Transport and Instability Phenomena*. Braun.